

# Studying the validity of relativistic hydrodynamics with a new exact solution of the Boltzmann equation

Gabriel Denicol

*Department of Physics, McGill University,  
3600 University Street, Montreal, QC H3A 2T8, Canada*

Ulrich Heinz and Mauricio Martinez

*Department of Physics, The Ohio State University, Columbus, OH 43210, USA*

Jorge Noronha

*Instituto de Física, Universidade de São Paulo,  
C.P. 66318, 05315-970 São Paulo, SP, Brazil*

Michael Strickland

*Physics Department, Kent State University, OH 44242 United States*

(Dated: March 2, 2022)

## Abstract

We present an exact solution to the Boltzmann equation which describes a system undergoing boost-invariant longitudinal and azimuthally symmetric radial expansion for arbitrary shear viscosity to entropy density ratio. This new solution is constructed by considering the conformal map between Minkowski space and the direct product of three dimensional de Sitter space with a line. The resulting solution respects  $SO(3)_q \otimes SO(1,1) \otimes Z_2$  symmetry. We compare the exact kinetic solution with exact solutions of the corresponding macroscopic equations with the same symmetry that were obtained from the kinetic theory in ideal and second-order viscous hydrodynamic approximations.

PACS numbers: 12.38.Mh, 24.10.Nz, 25.75.-q, 51.10.+y, 52.27.Ny

Keywords: Relativistic hydrodynamics, relativistic transport, relativistic kinetic theory, Boltzmann equation

## I. INTRODUCTION

One of the most important cornerstones of statistical physics is the Boltzmann equation. This equation has been extremely useful in describing the behavior and transport properties of a dilute gas in terms of its intrinsic microscopic dynamics. The Boltzmann equation is a partial differential equation with a very rich and complex mathematical structure which makes it difficult to solve it exactly by analytical means. There are very few exact solutions to the Boltzmann equation in the scientific literature. As a matter of fact, even for classical systems, the problem of the existence and uniqueness of solutions to this kinetic equation has not been completely sorted out for any collision kernel except in some particular cases [1]. Due to these limitations, there have been different expansion schemes put forward in the literature that allow one to obtain approximate solutions to the Boltzmann equation. Among the most important approaches are the Chapman-Enskog and Grad's moments methods [2]. The generalization of these methods to relativistic kinetic theory has been a source of debate since its foundations. For instance, at first order the Chapman-Enskog method [2, 3] leads to the relativistic Navier-Stokes (NS) equations which are acausal and unstable [4, 5]. To address this problem, Israel and Stewart (IS) [6] generalized Grad's original idea to the relativistic case to create a causal second order formulation of relativistic viscous hydrodynamics.<sup>1</sup> However, the original IS approach presents certain inconsistencies when obtaining the fluid dynamical equations using truncated approximations to the distribution function. A consistent framework has been developed recently in [10, 11]. Despite these advances, different approximation schemes can lead to different results for key physical quantities such as the transport coefficients [2, 12]. Exact solutions to the Boltzmann equation allow one to compare and characterize the effectiveness of the different approximation methods. In addition, an exact solution has the potential to shed light on the process of momentum isotropization in a non-equilibrated system.

There are also very few exact solutions to the hydrodynamic equations of motion. Recently, Gubser developed a method to construct exact solutions to the relativistic ideal and first order NS hydrodynamical approximations for a conformal fluid [13, 14] undergoing simultaneously boost-invariant longitudinal and azimuthally symmetric ("radial") transverse

---

<sup>1</sup> It is also possible to formulate higher-order relativistic viscous hydrodynamics using Chapman-Enskog like methods in the relaxation time approximation, see e.g. [7–9].

expansion (“Gubser flow”). The Gubser solution is based on powerful symmetry considerations: It is symmetric under the  $SO(3)_q \otimes SO(1, 1) \otimes Z_2$  group of transformations (“Gubser group”). In Minkowski coordinates this symmetry group is not explicitly manifest, and hence the strategy is to make use of the conformal map between Minkowski space and the curved spacetime formed by the direct product of a 3-dimensional de Sitter (dS) space with a line,  $dS_3 \otimes R$ , in which the Gubser symmetry *is* manifest [14]: A fluid that expands in Minkowski space with Gubser-symmetric flow looks static in  $dS_3 \otimes R$ . The equations of motion for the remaining hydrodynamic fields (temperature, energy density, etc.) are much simpler in de Sitter space than in Minkowski space and easily solved. Once the solutions are known in  $dS_3 \otimes R$ , it is straightforward to transform them back to Minkowski space. This yields a 1-parameter set of velocity and temperature profiles with non-trivial radial and time dependence, characterized by a single overall scale parameter [13, 14].

Recently, Gubser’s solution was extended to second-order conformal IS hydrodynamics [15]. Furthermore, the authors of [16, 17] generalized Gubser’s original approach by considering more general conformal maps between Minkowski space and other curved spaces, resulting in exact solutions including vorticity and associated dissipative corrections to ideal hydrodynamics.

In this work we discuss how to carry out a similar program for kinetic theory. If a very densely populated system is invariant under a certain group of symmetries, it is natural to ask how this symmetry becomes manifest in the one-particle distribution function. For instance, if there is homogeneity along a certain direction, say along the  $x$  axis, this means that the distribution function  $f(x^\mu, p_i) = f(t, y, z; p_i)$ , *i.e.* it does not depend on  $x$  and the number of independent variables on which the solution of the Boltzmann equation can depend has correspondingly been reduced by one. One can guess that eventually, if the system has enough symmetries, it must be possible to solve the Boltzmann equation exactly. In the context of ultrarelativistic heavy-ion collisions, this strategy was first discussed by Baym [18] who solved the Boltzmann equation exactly using the relaxation time approximation (RTA) for the collisional kernel.<sup>2</sup> In this case, longitudinal boost-invariance and invariance under translations in the transverse plane were the only ingredients necessary to obtain the exact solution. It describes a transversely homogeneous system expanding along the

---

<sup>2</sup> See also Refs. [19–21] for recent extensions to conformal and non-conformal systems.

longitudinal direction with the boost-invariant (scaling) flow profile discovered by Bjorken [22]. Despite its beauty and simplicity, this solution has limited applications since the spacetime dynamics of any spatially finite system is affected by transverse expansion, with highly nontrivial and experimentally observable consequences.

Gubser’s important achievement was to generalize Bjorken’s macroscopic hydrodynamic solution to systems undergoing additionally transverse expansion. In this paper we show how this generalization can be extended to the microscopic level, by solving the Boltzmann equation with RTA collision term exactly for systems with Gubser symmetry that undergo simultaneous boost-invariant longitudinal and azimuthally symmetric transverse expansion. Our solution can be used to describe systems with any value of the shear viscosity to entropy density ratio  $\eta/\mathcal{S}$ , and the result can be used to test the efficiency of various macroscopic (hydrodynamic) approximation methods. In addition, it can help us to understand the dynamics of the isotropization/thermalization process in anisotropically expanding systems with different longitudinal and transverse expansion rates.

Some of the ideas presented in this work were already introduced by us in a previous publication [23]. In this paper we present a more detailed derivation of our exact solution as well as an extended discussion of our findings. The paper is organized as follows. In Sec. II we present a short overview of the exact Gubser solution of conformal hydrodynamics. In Sec. III we discuss the necessary aspects of the Boltzmann equation in a curved spacetime. In Sec. IV we present the main result of this work, our new exact solution to the Boltzmann equation for a conformal system with Gubser symmetry. In this section we also describe how to recover first- and second-order conformal hydrodynamics from the exact solution of the Boltzmann equation. In Sec. V we discuss some aspects of the exact solution, illustrate it graphically, and make comparisons with the predictions of different approximation methods for solving the Boltzmann equation. Our conclusions are summarized in Sec. VI.

Before proceeding to the body of this work, let us define our metric conventions and notations. The metric signature is taken to be “mostly plus”: in Minkowski space the spacetime distance between two events is written in Cartesian coordinates  $x^\mu = (t, \mathbf{x})$  as

$$ds^2 = g_{\mu\nu}x^\mu x^\nu = -dt^2 + dx^2 + dy^2 + dz^2. \quad (1)$$

With this signature convention the flow velocity  $u^\mu$  is normalized as  $u_\mu u^\mu = -1$ . Milne coordinates in Minkowski space are defined by  $x^\mu = (\tau, x, y, \varsigma)$ , with longitudinal proper time

$\tau = \sqrt{t^2 - z^2}$ , spacetime rapidity  $\varsigma = \tanh^{-1}(z/t)$ , and metric  $ds^2 = -d\tau^2 + dx^2 + dy^2 + \tau^2 d\varsigma^2$ . Polar coordinates in the transverse plane are defined as usual by  $r = \sqrt{x^2 + y^2}$  and  $\phi = \tan^{-1}(y/x)$ . We denote the scalar product between two four-vectors with a dot, *i.e.*  $A_\mu B^\mu \equiv A \cdot B$ .

## II. THE GUBSER SOLUTION OF CONFORMAL HYDRODYNAMICS

In this section we briefly review the techniques introduced by Gubser [13] to find exact solutions for conformally invariant relativistic fluid dynamics. For a more complete discussion we refer the reader to the original works [13, 14]. The material discussed in this section provides the necessary background for our analogous treatment of the Boltzmann equation in Sec. III.

Gubser's exact solution to the conformal hydrodynamic equations respects  $SO(3)_q \otimes SO(1,1) \otimes Z_2$  symmetry. The  $SO(3)_q$  group reflects invariance under rotations in the transverse plane coupled with two special conformal transformations. In the Minkowski coordinates  $x^\mu = (\tau, r, \phi, \varsigma)$  the generators of  $SO(3)_q$  are given by [13]

$$\xi_1 = 2q^2 \tau r \cos \phi \frac{\partial}{\partial(q\tau)} + (1 + q^2 \tau^2 + q^2 r^2) \cos \phi \frac{\partial}{\partial(qr)} - \frac{1 + q^2 \tau^2 - q^2 r^2}{qr} \sin \phi \frac{\partial}{\partial \phi}, \quad (2a)$$

$$\xi_2 = 2q^2 \tau r \sin \phi \frac{\partial}{\partial(q\tau)} + (1 + q^2 \tau^2 + q^2 r^2) \sin \phi \frac{\partial}{\partial(qr)} + \frac{1 + q^2 \tau^2 - q^2 r^2}{qr} \cos \phi \frac{\partial}{\partial \phi}, \quad (2b)$$

$$\xi_3 = \frac{\partial}{\partial \phi}. \quad (2c)$$

Here  $q$  is an arbitrary energy scale; the solution is invariant under a change of  $q$  if simultaneously its transverse radius  $r$  and the longitudinal proper time  $\tau$  are rescaled by  $1/q$ . Invariance under  $SO(1,1)$  translates into boost invariance along the longitudinal axis and its generator is simply  $\partial/\partial \varsigma$ . The  $Z_2$  invariance is associated with longitudinal reflection symmetry under  $\varsigma \rightarrow -\varsigma$ .

It is not straightforward to obtain the flow velocity profile from the  $SO(3)_q$  generators (2) in Minkowski space. However, the flow is naturally understood [13, 14] in the curved spacetime  $dS_3 \otimes R$  which is related to Minkowski space via a Weyl-rescaling of the metric:

$$d\hat{s}^2 = \frac{ds^2}{\tau^2} = \frac{-d\tau^2 + dx^2 + dy^2}{\tau^2} + d\varsigma^2 = \frac{-d\tau^2 + dr^2 + r^2 d\phi^2}{\tau^2} + d\varsigma^2. \quad (3)$$

If one parametrizes the variables  $(\tau, r)$  in terms of new coordinates  $(\rho, \theta)$  defined by

$$\rho(\tau, r) = -\operatorname{arcsinh} \left( \frac{1 - q^2 \tau^2 + q^2 r^2}{2q\tau} \right), \quad (4a)$$

$$\theta(\tau, r) = \arctan \left( \frac{2qr}{1 + q^2 \tau^2 - q^2 r^2} \right), \quad (4b)$$

then the measure (3) becomes

$$d\hat{s}^2 = -d\rho^2 + \cosh^2 \rho (d\theta^2 + \sin^2 \theta d\phi^2) + d\varsigma^2, \quad (5)$$

with metric  $\hat{g}_{\mu\nu} = \operatorname{diag}(-1, \cosh^2 \rho, \cosh^2 \rho \sin^2 \theta, 1)$ . In the new coordinate system  $(\rho, \theta, \phi, \varsigma)$  the  $SO(3)_q$  conformal symmetry is manifest since the measure (5) is invariant under rotations of the sphere parametrized by  $(\theta, \phi)$ . In these coordinates, the generators of the  $SO(3)_q$  group are given by

$$\xi_1 = 2 \left( \cos \phi \frac{\partial}{\partial \theta} - \cot \theta \sin \phi \frac{\partial}{\partial \phi} \right), \quad (6a)$$

$$\xi_2 = 2 \left( \sin \phi \frac{\partial}{\partial \theta} + \cot \theta \cos \phi \frac{\partial}{\partial \phi} \right), \quad (6b)$$

$$\xi_3 = \frac{\partial}{\partial \phi}, \quad (6c)$$

which are precisely the well known angular momentum generators. In this paper, all quantities in de Sitter coordinates are denoted with a hat.

In  $dS_3 \otimes R$ , it is straightforward to see that the flow velocity  $\hat{u}_\mu = (-1, 0, 0, 0)$  is completely invariant under the  $SO(3)_q$  generators (6).<sup>3</sup> In order to obtain the velocity profile in Minkowski space we simply have to map back from the coordinate system  $\hat{x}^\mu = (\rho, \theta, \phi, \varsigma)$  to  $x^\mu = (\tau, r, \phi, \varsigma)$ , combined with the appropriate Weyl rescaling of the fluid velocity [14]:

$$u_\mu = \tau \frac{\partial \hat{x}^\nu}{\partial x^\mu} \hat{u}_\nu. \quad (7)$$

This results in the following expressions for the Milne components of the fluid four-velocity  $u_\mu$  in Minkowski space [13, 14]:

$$u_\tau = -\cosh \kappa(\tau, r), \quad u_r = \sinh \kappa(\tau, r), \quad u_\phi = u_\varsigma = 0, \quad (8)$$

---

<sup>3</sup> This can be compared with the Bjorken flow solution where  $u_\mu \equiv (u_\tau, u_r, u_\phi, u_\varsigma) = (-1, 0, 0, 0)$  appears as the only time-like unit vector that is invariant (*i.e.* has zero Lie derivative) under translations  $\frac{\partial}{\partial x}$ ,  $\frac{\partial}{\partial y}$  in the transverse plane, boosts  $\frac{\partial}{\partial \varsigma}$ , and rotations  $\frac{\partial}{\partial \phi}$  around the beam axis ( $z$  direction). Therefore, the temperature and any other hydrodynamical variables become functions of  $\tau$  only.

with the transverse flow rapidity

$$\kappa(\tau, r) = \tanh^{-1} \left( \frac{2q^2 \tau r}{1 + q^2 \tau^2 + q^2 r^2} \right). \quad (9)$$

In de Sitter space the ideal hydrodynamic equations reduce to a single continuity equation for the thermal equilibrium energy density  $\hat{\varepsilon}$ . For dissipative hydrodynamics one has to solve in addition an equation of motion for the shear-stress tensor  $\hat{\pi}^{\mu\nu}$ . Some aspects of the dissipative IS solution are discussed in Appendix A; for a more complete discussion we direct the interested reader to Ref. [15]. From the solutions for the hydrodynamical fields in de Sitter space one obtains the non-trivial solution in Minkowski space through the transformation rules [13, 14]

$$\varepsilon(\tau, r) = \frac{\hat{\varepsilon}(\rho(\tau, r))}{\tau^4}, \quad (10a)$$

$$\pi_{\mu\nu}(\tau, r) = \frac{1}{\tau^2} \frac{\partial \hat{x}^\alpha}{\partial x^\mu} \frac{\partial \hat{x}^\beta}{\partial x^\nu} \hat{\pi}_{\alpha\beta}(\rho(\tau, r)). \quad (10b)$$

### III. RELATIVISTIC BOLTZMANN EQUATION IN CURVED SPACES

The general relativistic Boltzmann equation for the *on-shell* one-particle distribution function is given by [3, 24, 25]

$$p^\mu \partial_\mu f + \Gamma_{\mu i}^\lambda p_\lambda p^\mu \frac{\partial f}{\partial p_i} = \mathcal{C}[f], \quad (11)$$

where the distribution function  $f = f(x^\mu, p_i)$  is defined in a 7-dimensional phase space. A point in this phase-space is described by seven coordinates, the spacetime coordinates  $x^\mu = (t, x, y, z)$  and the three spatial covariant momentum components  $p_i = (p_x, p_y, p_z)$ . The zero component of the momentum is obtained from the on-shell condition  $p_0 = p_0(x^\lambda, p_i)$ . Moreover, in Eq. (11) the Christoffel symbol  $\Gamma_{\mu i}^\lambda$  is defined as<sup>4</sup>

$$\Gamma_{\mu\nu}^\lambda = \frac{g^{\lambda\beta}}{2} (\partial_\mu g_{\beta\nu} + \partial_\nu g_{\beta\mu} - \partial_\beta g_{\mu\nu}). \quad (12)$$

Equation (11) is covariant under general coordinate transformations  $x^\mu \rightarrow \hat{x}^\mu(x^\lambda)$ , although not manifestly so [24, 25]. There are other ways to write this equation where the general

---

<sup>4</sup> For a general curved spacetime the Christoffel symbols are non vanishing but they can also be nonzero for a given flat spacetime depending on the choice of coordinates. For instance when parametrizing any vector  $x^\mu$  in Minkowski space by using Milne coordinates  $x^\mu = (\tau, x, y, \varsigma)$ , the Christoffel symbols with nonzero components are  $\Gamma_{\varsigma\varsigma}^\tau = \tau$  and  $\Gamma_{\tau\tau}^\varsigma = \Gamma_{\tau\varsigma}^\varsigma = 1/\tau$ .

coordinate covariance is explicit [25]. For instance, one can define an off-shell distribution  $F(x^\mu, p_\mu)$  that satisfies a manifestly covariant Boltzmann equation [24, 25]. We will not make use of this approach since the form of Eq. (11) is more convenient for our purposes. The explicit form of the collision term on the right-hand side for  $2 \leftrightarrow 2$  scattering can be found in [24, 25]. In this work, we restrict ourselves to a simple approximation for the collisional kernel, the relaxation time approximation (RTA), in which  $\mathcal{C}[f]$  is given by [26, 27]

$$\mathcal{C}[f] = \frac{p \cdot u}{\tau_{\text{rel}}} [f(x^\mu, p_i) - f_{\text{eq}}(x^\mu, p_i)]. \quad (13)$$

Here  $u^\mu$  is the fluid velocity,  $T$  is the temperature in the local rest frame,  $\tau_{\text{rel}}$  is the relaxation time which can depend on proper time,  $f_{\text{eq}}(x^\mu, p_i) = f_{\text{eq}}(p \cdot u/T)$  is the local equilibrium Jüttner distribution, and the fluid velocity is defined in the Landau frame.

For a given distribution function  $f(x^\mu, p_i)$  one obtains the energy-momentum tensor  $T^{\mu\nu}$  as the following moment of the distribution function [2, 3]:

$$T^{\mu\nu}(x) = \int \frac{d^3p}{(2\pi)^3 \sqrt{-g} p^0} p^\mu p^\nu f(x^\mu, p_i). \quad (14)$$

The relevant macroscopic variables such as the energy density, pressure, etc., are most easily identified by decomposing the four-momentum into temporal and spatial parts *in the local rest frame*,  $p^\mu = -(u \cdot p)u^\mu + \Delta^{\mu\nu}p_\nu$ , where  $-u^\mu u^\nu$  and  $\Delta^{\mu\nu} = g^{\mu\nu} + u^\mu u^\nu$  are the projectors parallel and orthogonal to  $u^\mu$ . Given this vector decomposition, the energy-momentum tensor (14) for a theory with vanishing bulk viscosity (as is the case in a conformal theory) can be written as

$$T^{\mu\nu}(x) = \varepsilon(x)u^\mu u^\nu + \Delta^{\mu\nu}\mathcal{P}(x) + \pi^{\mu\nu}(x), \quad (15)$$

where  $\varepsilon$  is the energy density,  $\mathcal{P}$  is the thermodynamic pressure, and  $\pi^{\mu\nu}$  is the shear-stress tensor which is traceless, symmetric, and orthogonal to the fluid velocity. The macroscopic quantities above can be obtained as momentum moments of an arbitrary distribution function [3]:

$$\varepsilon(x) = \int \frac{d^3p}{(2\pi)^3 \sqrt{-g} p^0} (p \cdot u)^2 f(x^\mu, p_i), \quad (16a)$$

$$\mathcal{P}(x) = \frac{1}{3} \int \frac{d^3p}{(2\pi)^3 \sqrt{-g} p^0} \Delta_{\mu\nu} p^\nu p^\mu f(x^\mu, p_i), \quad (16b)$$

$$\pi^{\mu\nu}(x) = \int \frac{d^3p}{(2\pi)^3 \sqrt{-g} p^0} p^{\langle\mu} p^{\nu\rangle} f(x^\mu, p_i). \quad (16c)$$



In Eq. (16c) we introduce the notation  $p^{\langle\mu}p^{\nu\rangle} = \Delta_{\alpha\beta}^{\mu\nu}p^\alpha p^\beta$  where the double projector  $\Delta_{\alpha\beta}^{\mu\nu} = (\Delta_\alpha^\mu \Delta_\beta^\nu + \Delta_\beta^\mu \Delta_\alpha^\nu - \frac{2}{3}\Delta^{\mu\nu}\Delta_{\alpha\beta})/2$  selects the traceless and orthogonal (to  $u^\mu$ ) part of a tensor. We will make use of these relations in Sec. IV to study the dynamics of the macroscopic variables for a distribution function that exactly solves the RTA Boltzmann equation with Gubser symmetry.

### A. The RTA Boltzmann equation in Milne coordinates

For a system with boost-invariant longitudinal expansion it is convenient to use Milne coordinates  $x^\mu = (\tau, x, y, \varsigma)$  with metric  $g_{\mu\nu} = \text{diag}(-1, 1, 1, \tau^2)$ . In this coordinate system the RTA Boltzmann equation (11) is written as (see footnote 4)

$$p^\tau \partial_\tau f + p_x \partial_x f + p_y \partial_y f + \frac{p_\varsigma}{\tau^2} \partial_\varsigma f = \frac{p \cdot u}{\tau_{\text{rel}}} (f - f_{\text{eq}}). \quad (17)$$

The on-shell condition allows us to determine  $p^\tau$ :

$$p_\mu p_\nu g^{\mu\nu} = -m^2 \implies p^\tau = \sqrt{m^2 + p_x^2 + p_y^2 + p_\varsigma^2/\tau^2}. \quad (18)$$

Since the Gubser symmetry to be studied in the following Section embodies conformal invariance which would be broken by non-zero mass terms, we set all masses to zero in this work.

### B. Emergent Weyl invariance in the massless limit

Building on recent work on Weyl invariant hydrodynamics [28] for systems close to local equilibrium, we here use similar techniques to study their non-equilibrium dynamics, as described by the Boltzmann equation. We start by showing that, for massless particles, conformal transformations are a symmetry of the Boltzmann equation in the RTA approximation.

Under a Weyl transformation, the metric changes as

$$g_{\mu\nu}(x) \rightarrow e^{-2\Omega(x)} g_{\mu\nu}(x), \quad (19)$$

where  $\Omega(x)$  is an arbitrary scalar function. A Weyl rescaling is not a general coordinate

transformation: The Ricci scalar changes, so a flat space transforms into a curved space.<sup>5</sup> This transformation is similar to the Mercator projection map used in cartography which maps the surface of the earth to a plane. Under a Weyl rescaling, a  $(m, n)$  tensor  $Q_{\nu_1 \dots \nu_n}^{\mu_1 \dots \mu_m}$  transforms as follows [28]:

$$Q_{\nu_1 \dots \nu_n}^{\mu_1 \dots \mu_m}(x) \rightarrow e^{(\Delta+m-n)\Omega(x)} Q_{\nu_1 \dots \nu_n}^{\mu_1 \dots \mu_m}(x), \quad (20)$$

where  $\Delta$  is its canonical dimension,  $m$  is the number of contravariant indices, and  $n$  is the number of covariant indices. For example, the velocity vector transforms as  $u_\mu \rightarrow e^{-\Omega} u_\mu$ ,  $u^\mu \rightarrow e^\Omega u^\mu$  while the temperature transforms as  $T \rightarrow e^\Omega T$ . Scalar products of four-vectors transform with the sum of their canonical dimensions.

Note that, to prove the Weyl covariance of the Boltzmann equation (11) we note that, consistent with its interpretation as a probability density in phase-space, the distribution function  $f(x^\mu, p_i)$  in Eq. (11) is a scalar with zero canonical dimension and thus invariant under Weyl transformations. Since for a conformal system  $\tau_{\text{rel}} \sim 1/T$ , the RTA collision term (13) on the r.h.s. of the Boltzmann equation (11) transforms homogeneously as  $\mathcal{C}[f] \rightarrow e^{2\Omega} \mathcal{C}[f]$  (as argued in [28] for a general collision term). Given (20), the first term on the l.h.s. of Eq. (11) and the term multiplied by the Christoffel symbol are seen to transform in the same way:  $p^\mu \partial_\mu f \rightarrow e^{2\Omega} p^\mu \partial_\mu f$  and  $p_\lambda p^\mu \frac{\partial f}{\partial p_i} \rightarrow e^{2\Omega} p_\lambda p^\mu \frac{\partial f}{\partial p_i}$ . However, the Christoffel symbol  $\Gamma_{\mu i}^\lambda$  itself transforms non-trivially under a Weyl rescaling:

$$\Gamma_{\mu\nu}^\lambda \rightarrow \Gamma_{\mu\nu}^\lambda - (g_\nu^\lambda \partial_\mu \Omega + g_\mu^\lambda \partial_\nu \Omega - g_{\mu\nu} \partial^\lambda \Omega). \quad (21)$$

This leads to an additional term on the l.h.s. of the Boltzmann equation (11):

$$\begin{aligned} (g_i^\lambda \partial_\mu \Omega + g_\mu^\lambda \partial_i \Omega - g_{\mu i} \partial^\lambda \Omega) p_\lambda p^\mu \frac{\partial f}{\partial p_i} &= (p_i p \cdot \partial \Omega + \partial_i \Omega p \cdot p - p_i p \cdot \partial \Omega) \frac{\partial f}{\partial p_i} \\ &= p \cdot p \partial_i \Omega \frac{\partial f}{\partial p_i}. \end{aligned} \quad (22)$$

This term vanishes identically if and only if the particles are massless, *i.e.* if  $p \cdot p = 0$ . Under these conditions one sees that the entire Boltzmann equation transforms homogeneously with  $e^{2\Omega}$  under Weyl rescaling:

$$p^\mu \partial_\mu f + \Gamma_{\mu i}^\lambda p_\lambda p^\mu \frac{\partial f}{\partial p_i} - \mathcal{C}[f] = 0 \implies e^{2\Omega} \left( p^\mu \partial_\mu f + \Gamma_{\mu i}^\lambda p_\lambda p^\mu \frac{\partial f}{\partial p_i} - \mathcal{C}[f] \right) = 0. \quad (23)$$

<sup>5</sup> A specific example was discussed in Sect. II: Due to the global factor  $1/\tau^2$ , the measure  $d\hat{s}^2$  in (3) does not parametrize standard Minkowski space  $R^3 \otimes R$ .

In the massless limit, the microscopic dynamics encoded in the distribution function thus possesses an “emergent” Weyl invariance, and conformal transformations from Minkowski to curved spaces are then indeed symmetries of the Boltzmann equation. In the following Section we will obtain an exact solution of the RTA Boltzmann equation by exploiting the conformal map between Minkowski space and  $dS_3 \otimes R$ .

### C. Solving the Boltzmann equation with Bjorken symmetry

Before doing so we would like to return to the case of boost invariant longitudinal expansion with translational and rotational symmetry in the transverse plane studied by Bjorken [22]. Transverse homogeneity implies that the distribution function  $f(x^\mu, p_i)$  cannot depend on the transverse coordinates  $x$  and  $y$ , while azimuthal symmetry around the longitudinal axis stipulates that any dependence on the transverse momentum components can be only through  $p_T = \sqrt{p_x^2 + p_y^2}$ . Longitudinal boost invariance implies that any time dependence of  $f$  can only occur in terms of the longitudinal proper time  $\tau = \sqrt{t^2 - z^2}$ , and that any dependence on the longitudinal position  $z$  and the longitudinal momentum component  $p_z$  must come in the boost invariant combination<sup>6</sup>

$$w = tp_z - zE. \quad (24)$$

We see that longitudinal boost invariance imposes strong constraints on the number of independent variables of the distribution function and on the particular combination in which the dependent variables appear [18–21, 29–31]. As we shall see in the following section, identifying these independent combinations of phase-space variables will be the key step in deriving the exact solution of the Boltzmann equation for an  $SO(3)_q \otimes SO(1, 1) \otimes Z_2$  symmetric system.

With the above simplifications the RTA Boltzmann equation (11) reduces to [18–21]

$$\partial_\tau f = -\frac{1}{\tau_{\text{rel}}(\tau)}(f - f_{\text{eq}}) \quad (25)$$

---

<sup>6</sup> The Lorentz  $\gamma$  factor for the Bjorken flow profile  $v_z = z/t$  is  $\gamma = (1 - v_z^2)^{-1/2} = t/\tau$ . A particle with momentum  $p_z$  at position  $z$  in the lab frame thus has momentum  $p'_z = \gamma(p_z - Ev) = (tp_z - Ez)/\tau \equiv w/\tau$  in the local rest frame. Since the physics in the local rest frame, in particular the  $p'_z$  distribution, is supposed to be independent of  $z$ ,  $f$  can depend on  $z$  and  $p_z$  only through  $w$ .

where  $f = f(\tau; p_T, w)$ . Its general solution for a momentum-independent relaxation time  $\tau_{\text{rel}}$  is given by

$$f(\tau; p_T, w) = D(\tau, \tau_0) f_0(p_T, w) + \int_{\tau_0}^{\tau} \frac{d\tau'}{\tau_{\text{rel}}(\tau')} D(\tau, \tau') f_{\text{eq}}(\tau'; p_T, w), \quad (26)$$

where  $D(\tau_2, \tau_1)$  is the damping function given by

$$D(\tau_2, \tau_1) = \exp\left(-\int_{\tau_1}^{\tau_2} \frac{d\tau''}{\tau_{\text{rel}}(\tau'')}\right), \quad (27)$$

and  $f_0(p_T, w)$  is the initial distribution function at  $\tau = \tau_0$  [18–21, 29–31]. In the past, different authors considered an equilibrium initial condition  $f_0(p_T, w) = f_{\text{eq}}(\tau_0; p_T, w)$  [18, 29–31]. Recently Florkowski *et al.* [19, 20] relaxed this assumption and studied a more general set of initial profiles for  $f_0$ , corresponding to an initially anisotropic local momentum distribution. The approach of Florkowski *et al.* has proven very useful since it allows one to test different viscous and anisotropic hydrodynamic approximation schemes [32–45] against the underlying microscopic Boltzmann dynamics, for both massless [19, 20] and massive cases [21].<sup>7</sup>

## IV. EXACT SOLUTION OF THE RTA BOLTZMANN EQUATION WITH GUBSER SYMMETRY

### A. The solution

We now discuss the consequences for the microscopic kinetic evolution of the system of requiring invariance under  $SO(3)_q \otimes SO(1, 1) \otimes Z_2$  transformations. The previous Section taught us that this is most easily studied in a coordinate system where the fluid is at rest. In addition, one should use a spacetime where the group symmetries are explicitly manifest. Hence, as pointed out in Sec. II, the most natural choice is to use the space  $dS_3 \otimes R$  parametrized by coordinates  $\hat{x}^\mu = (\rho, \theta, \phi, \varsigma)$ .

As in the case of Bjorken symmetry, the Gubser symmetry severely restricts the combinations of the coordinates  $\hat{x}^\mu = (\rho, \theta, \phi, \varsigma)$  and momenta  $\hat{p}_i = (\hat{p}_\theta, \hat{p}_\phi, \hat{p}_\varsigma)$  on which  $f(\hat{x}^\mu, \hat{p}_i)$  can depend. Each of the three factors of the Gubser group  $SO(3)_q \otimes SO(1, 1) \otimes Z_2$  imposes its own constraints:

---

<sup>7</sup> We point out that the solution (26) for the distribution function was derived using only the symmetry constraints, without assumptions about the particle mass [18]. This will be different for the case of Gubser symmetry studied in the following Section.

- The generators of  $SO(3)_q$  describe rotations of spatial vectors parametrized by the  $(\theta, \phi)$  variables, and simultaneously of momentum vectors parametrized by the coordinates  $(\hat{p}_\theta, \hat{p}_\phi)$ , over a sphere  $S^2$ .  $SO(3)_q$  symmetry demands that physical observables (such as the distribution function  $f$ ) can only depend on the following  $SO(3)_q$ -invariant combination of these four variables:

$$\hat{p}_\Omega^2 = \hat{p}_\theta^2 + \frac{\hat{p}_\phi^2}{\sin^2 \theta}. \quad (28)$$

Geometrically  $\hat{p}_\Omega^2$  is the radius of the sphere  $S^2$  in  $(\hat{p}_\theta, \hat{p}_\phi)$  momentum-space coordinates.<sup>8</sup> Thus, we interpret  $\hat{p}_\Omega$  as the total momentum associated with the momentum components  $(\hat{p}_\theta, \hat{p}_\phi)$ .

- The  $SO(1, 1)$  invariance imposes the same constraints on the distribution function as previously discussed in Sec. III C for the case of Bjorken symmetry: in Milne coordinates, the distribution function depends only on the proper time  $\tau$ , the transverse momentum  $p_T$  and the variable  $w$  (24), but not on the spatial rapidity  $\varsigma$ . The  $SO(3)_q$  symmetry modifies the dependence on the first two variables ( $\tau$  and  $p_T$ ) in de Sitter space. Given the conformal map between Minkowski and de Sitter space one can show that the variable  $w$  is related to the  $\hat{p}_\varsigma$  component.<sup>9</sup> Therefore, the  $SO(1, 1)$  invariance implies that, in addition to  $\hat{p}_\Omega$ , the distribution function can depend in momentum space only on  $\hat{p}_\varsigma$ .
- The  $Z_2$  invariance implies that the distribution function is invariant under reflection  $\varsigma \rightarrow -\varsigma$ .

<sup>8</sup> This situation is analogous to what happens in the hydrogen atom problem in quantum mechanics. There, the only combination of the generators  $L_x$ ,  $L_y$  and  $L_z$  of the  $SO(3)$  angular momentum algebra with which all three generators commute is the Casimir operator  $L^2 = L_x^2 + L_y^2 + L_z^2$ .

<sup>9</sup> The covariant components of the momentum transform as [3]

$$p'^\mu = \frac{\partial x'^\mu}{\partial x^\nu} p^\nu. \quad (29)$$

When transforming from  $(t, x, y, z)$  to  $(\tau, x, y, \varsigma)$  coordinates, this prescription yields for the  $\varsigma$ -component of the momentum the expression

$$p^\varsigma = \frac{1}{\tau^2} (tp^z - zp^0) = \frac{w}{\tau^2} = \frac{p_\varsigma}{\tau^2},$$

where we used the definition (24) of the variable  $w$ . Under Weyl rescaling (7) this component transforms into  $\hat{p}^\varsigma = \tau^2 p^\varsigma = p_\varsigma = \hat{p}_\varsigma = w$ . Note that under a boost with rapidity  $\varsigma_{boost}$ ,  $\varsigma \rightarrow \varsigma + \varsigma_{boost}$  while  $\hat{p}^\varsigma$  remains invariant.

As a result of these considerations we see that the conformal symmetry group demands that  $f(\hat{x}^\mu, \hat{p}_i) = f(\rho; \hat{p}_\Omega^2, \hat{p}_\varsigma)$ . Its only dependence on the spacetime coordinates is through the “de Sitter time”  $\rho$ . Conformality also imposes constraints on the functional dependence of the relaxation time on the temperature:  $\tau_{\text{rel}} = c/T$  where  $c$  is a free dimensionless parameter related to the shear viscosity to entropy density ratio  $\eta/\mathcal{S}$ . For the RTA collision kernel used in this work one has [10, 19, 20, 46]

$$c = \frac{5\eta}{\mathcal{S}} \iff \frac{\eta}{\mathcal{S}} = \frac{1}{5} \tau_{\text{rel}} T, \quad (30)$$

where  $\eta$  is the shear viscosity and  $\mathcal{S}$  the entropy density. Due to the conformal map between Minkowski space and  $dS_3 \otimes R$  one has the relation

$$T(\tau, r) = \hat{T}(\rho(\tau, r))/\tau. \quad (31)$$

Putting all these ingredients together, Gubser invariance is seen to greatly simplify the RTA Boltzmann equation (17). Starting with the RTA Boltzmann equation in Milne coordinates, changing the variables from  $x^\mu \rightarrow \hat{x}^\mu$  and performing the necessary Weyl rescalings, one finds that the kinetic equation can be written in  $dS_3 \otimes R$  coordinates as

$$\frac{\partial}{\partial \rho} f(\rho; \hat{p}_\Omega^2, \hat{p}_\varsigma) = -\frac{\hat{T}(\rho)}{c} \left[ f(\rho; \hat{p}_\Omega^2, \hat{p}_\varsigma) - f_{\text{eq}}(\hat{p}^\rho / \hat{T}(\rho)) \right], \quad (32)$$

where  $\hat{p}^\rho$  is determined from the massless on-shell condition

$$\hat{p}^\rho = \sqrt{\frac{\hat{p}_\Omega^2}{\cosh^2 \rho} + \hat{p}_\varsigma^2}. \quad (33)$$

Comparing Eqs. (32) and (25), the solution for  $f(\rho; \hat{p}_\Omega^2, \hat{p}_\varsigma)$  is easily found:

$$f(\rho; \hat{p}_\Omega^2, \hat{p}_\varsigma) = D(\rho, \rho_0) f_0(\rho_0; \hat{p}_\Omega^2, \hat{p}_\varsigma) + \frac{1}{c} \int_{\rho_0}^{\rho} d\rho' D(\rho, \rho') \hat{T}(\rho') f_{\text{eq}}(\rho'; \hat{p}_\Omega^2, \hat{p}_\varsigma). \quad (34)$$

The damping function in this case is given by

$$D(\rho_2, \rho_1) = \exp\left(-\int_{\rho_1}^{\rho_2} d\rho'' \frac{\hat{T}(\rho'')}{c}\right). \quad (35)$$

In Eqs. (34) and (35),  $\rho_0$  is the initial “time” in de Sitter space at which  $f = f_0(\rho_0; \hat{p}_\Omega^2, \hat{p}_\varsigma)$ . In the present work we assume that  $f_0$  is given by a Boltzmann equilibrium distribution function at  $\rho_0$ . With this assumption the Weyl rescaling property is preserved for any value of the  $\rho$  variable.

## B. Energy-momentum tensor components

The solution (34) of the Boltzmann equation allows us to calculate the evolution of all components of the energy-momentum tensor from their definitions, Eqs. (16). For reference, let us first calculate the energy density for a Boltzmann equilibrium distribution function:

$$\begin{aligned}\hat{\varepsilon}_{\text{eq}}(\rho) &= \frac{1}{(2\pi)^3} \int_{-\infty}^{\infty} d\hat{p}_{\varsigma} \int_{-\infty}^{\infty} \frac{d\hat{p}_{\theta}}{\cosh \rho} \int_{-\infty}^{\infty} \frac{d\hat{p}_{\phi}}{\cosh \rho \sin \theta} \hat{p}^{\rho} e^{-\hat{p}^{\rho}/\hat{T}(\rho)} \\ &= \frac{3}{\pi^2} \hat{T}^4(\rho).\end{aligned}\tag{36}$$

As expected for a conformal theory,  $\hat{\varepsilon}_{\text{eq}} \sim \hat{T}^4$ . The energy density associated with the exact solution (34) of the Boltzmann equation is obtained as follows:

$$\begin{aligned}\hat{\varepsilon}(\rho) &= \frac{1}{(2\pi)^3} \int_{-\infty}^{\infty} d\hat{p}_{\varsigma} \int_{-\infty}^{\infty} \frac{d\hat{p}_{\theta}}{\cosh \rho} \int_{-\infty}^{\infty} \frac{d\hat{p}_{\phi}}{\cosh \rho \sin \theta} \hat{p}^{\rho} f(\rho; \hat{p}_{\Omega}^2, \hat{p}_{\varsigma}) \\ &= \frac{3}{\pi^2} \left[ D(\rho, \rho_0) \mathcal{H}\left(\frac{\cosh \rho_0}{\cosh \rho}\right) \hat{T}_0^4 + \frac{1}{c} \int_{\rho_0}^{\rho} d\rho' D(\rho, \rho') \mathcal{H}\left(\frac{\cosh \rho'}{\cosh \rho}\right) \hat{T}^5(\rho') \right],\end{aligned}\tag{37}$$

where in the last line we used both Eqs. (34) and (36). In Eq. (37)  $\hat{T}_0 \equiv \hat{T}(\rho_0)$ , and the function  $\mathcal{H}(x)$  is

$$\mathcal{H}(x) = \frac{1}{2} \left( x^2 + x^4 \frac{\tanh^{-1}(\sqrt{1-x^2})}{\sqrt{1-x^2}} \right).\tag{38}$$

It is straightforward to show that for the distribution function (34) the pressure (16b) is related to the energy density by the conformal equation of state  $\hat{\mathcal{P}}(\rho) = \hat{\varepsilon}(\rho)/3$  at all de Sitter times  $\rho$ .

From its definition, the shear stress tensor (16c) is

$$\hat{\pi}^{\mu\nu} = \frac{1}{(2\pi)^3} \int_{-\infty}^{\infty} d\hat{p}_{\varsigma} \int_{-\infty}^{\infty} \frac{d\hat{p}_{\theta}}{\cosh \rho} \int_{-\infty}^{\infty} \frac{d\hat{p}_{\phi}}{\cosh \rho \sin \theta} \frac{1}{\hat{p}^{\rho}} \hat{p}^{(\mu} \hat{p}^{\nu)} f(\rho; \hat{p}_{\Omega}^2, \hat{p}_{\varsigma})\tag{39}$$

In the  $(\rho, \theta, \phi, \varsigma)$  coordinate system the only nonzero components of the shear stress tensor are

$$\begin{aligned}\hat{\pi}_{\varsigma}^{\varsigma}(\rho) &= \frac{1}{(2\pi)^3} \int_{-\infty}^{\infty} d\hat{p}_{\varsigma} \int_{-\infty}^{\infty} \frac{d\hat{p}_{\theta}}{\cosh^2 \rho} \int_{-\infty}^{\infty} \frac{d\hat{p}_{\phi}}{\sin \theta} \frac{1}{\hat{p}^{\rho}} \left( \hat{p}_{\varsigma}^2 - \frac{(\hat{p}^{\rho})^2}{3} \right) f \\ &= \frac{1}{\pi^2} \left[ D(\rho, \rho_0) \mathcal{A}\left(\frac{\cosh \rho}{\cosh \rho_0}\right) \hat{T}_0^4 + \frac{1}{c} \int_{\rho_0}^{\rho} d\rho' D(\rho, \rho') \mathcal{A}\left(\frac{\cosh \rho}{\cosh \rho'}\right) \hat{T}^5(\rho') \right],\end{aligned}\tag{40a}$$

$$\hat{\pi}_{\theta}^{\theta}(\rho) = \frac{1}{(2\pi)^3} \int_{-\infty}^{\infty} d\hat{p}_{\varsigma} \int_{-\infty}^{\infty} \frac{d\hat{p}_{\theta}}{\cosh^2 \rho} \int_{-\infty}^{\infty} \frac{d\hat{p}_{\phi}}{\sin \theta} \frac{1}{\hat{p}^{\rho}} \left( \frac{\hat{p}_{\theta}^2}{\cosh^2 \rho} - \frac{(\hat{p}^{\rho})^2}{3} \right) f = -\frac{1}{2} \hat{\pi}_{\varsigma}^{\varsigma}(\rho),\tag{40b}$$

$$\hat{\pi}_{\phi}^{\phi}(\rho) = \frac{1}{(2\pi)^3} \int_{-\infty}^{\infty} d\hat{p}_{\varsigma} \int_{-\infty}^{\infty} \frac{d\hat{p}_{\theta}}{\cosh^2 \rho} \int_{-\infty}^{\infty} \frac{d\hat{p}_{\phi}}{\sin \theta} \frac{1}{\hat{p}^{\rho}} \left( \frac{\hat{p}_{\phi}^2}{\cosh^2 \rho \sin^2 \theta} - \frac{(\hat{p}^{\rho})^2}{3} \right) f = -\frac{1}{2} \hat{\pi}_{\varsigma}^{\varsigma}(\rho).\tag{40c}$$

Here  $f = f(\rho; \hat{p}_\Omega^2, \hat{p}_\zeta)$ , and we defined

$$\mathcal{A}(x) = \frac{x\sqrt{x^2-1}(1+2x^2) + (1-4x^2)\coth^{-1}(x/\sqrt{x^2-1})}{2x^3(x^2-1)^{3/2}}. \quad (41)$$

Clearly, these expressions are consistent with  $SO(3)_q$  symmetry which demands  $\hat{\pi}_\theta^\theta = \hat{\pi}_\phi^\phi$ , and with the tracelessness of the shear stress tensor,  $\hat{\pi}_\theta^\theta + \hat{\pi}_\phi^\phi + \hat{\pi}_\zeta^\zeta = 0$ . Eqs. (40) tell us that for a fluid undergoing Gubser flow [13–15] the shear stress tensor has only a single independent non-zero component for which we choose  $\hat{\pi}_\zeta^\zeta$ . One checks easily that, as expected, all shear stress components in (40) approach zero when  $f \rightarrow f_{\text{eq}}$ .

### C. Matching condition: definition of temperature

For any point  $\rho$ , we define the local temperature  $\hat{T}(\rho)$  of the fluid using the traditional matching condition

$$\hat{\varepsilon}(\rho) = \hat{\varepsilon}_{\text{eq}}(\hat{T}(\rho)) = \frac{3}{\pi^2} \hat{T}^4(\rho). \quad (42)$$

Inserting this into Eq. (37) we obtain the following integral equation for the temperature of the system:

$$\hat{T}^4(\rho) = D(\rho, \rho_0) \mathcal{H}\left(\frac{\cosh \rho_0}{\cosh \rho}\right) \hat{T}^4(\rho_0) + \frac{1}{c} \int_{\rho_0}^{\rho} d\rho' D(\rho, \rho') \mathcal{H}\left(\frac{\cosh \rho'}{\cosh \rho}\right) \hat{T}^5(\rho'). \quad (43)$$

This integral equation can be solved iteratively. Once  $\hat{T}(\rho)$  has been determined, it can be used to calculate from Eq. (34) the full distribution function and from Eq. (40a) the non-vanishing component of the shear stress tensor.

### D. Conformal hydrodynamics from the exact kinetic solution

In this subsection we show how to obtain first- [13, 14] and second-order [15] conformal viscous hydrodynamics from the exact solution (34) of the Boltzmann equation. To obtain the evolution equation for the viscous shear stress tensor one can follow the method described in [10, 11]. Our starting point is to rewrite the Boltzmann equation (32) in the following form

$$\frac{\partial \delta f}{\partial \rho} = -\frac{\delta f}{\hat{\tau}_{\text{rel}}(\rho)} - \frac{\partial f_{\text{eq}}}{\partial \rho}, \quad (44)$$



where  $\hat{\tau}_{\text{rel}}(\rho) = \tau_{\text{rel}}(\rho)/\tau = c/\hat{T}(\rho)$  and  $\delta f = f - f_{\text{eq}}$ . The general expression for the shear-stress tensor (16c) in terms of  $\delta f$  is

$$\hat{\pi}^{\langle\mu\nu\rangle} = \frac{1}{(2\pi)^3} \int \frac{d^3\hat{p}}{\sqrt{-g}\hat{p}^\rho} \hat{\Delta}_{\alpha\beta}^{\mu\nu} \hat{p}^\alpha \hat{p}^\beta \delta f. \quad (45)$$

Taking the derivative with respect to  $\rho$  we obtain the equation of motion

$$\partial_\rho \hat{\pi}^{\langle\mu\nu\rangle} = \hat{\Delta}_{\alpha\beta}^{\mu\nu} \frac{\partial}{\partial \rho} \hat{\pi}^{\alpha\beta} = \int \frac{d^3\hat{p}}{(2\pi)^3} \hat{\Delta}_{\alpha\beta}^{\mu\nu} \hat{p}^\alpha \hat{p}^\beta \left[ \frac{1}{\sqrt{-g}\hat{p}^\rho} \frac{\partial \delta f}{\partial \rho} + \delta f \frac{\partial}{\partial \rho} \left( \frac{1}{\sqrt{-g}\hat{p}^\rho} \right) \right], \quad (46)$$

where  $\hat{\Delta}_{\alpha\beta}^{\mu\nu}$  is the transverse and traceless double projector defined in  $dS_3 \otimes R$  with  $(\rho, \theta, \phi, \varsigma)$  coordinates. In this step all terms that vanish in the massless limit have been dropped. Using the Boltzmann equation (44) for  $\delta f$  together with  $f_{\text{eq}} = e^{-\hat{p}^\rho/\hat{T}(\rho)}$  one obtains the following (exact but implicit) evolution equation:

$$\begin{aligned} \partial_\rho \hat{\pi}^{\langle\mu\nu\rangle} = & -\frac{\hat{\pi}^{\mu\nu}}{\hat{\tau}_{\text{rel}}} - 2\hat{\pi}^{\mu\nu} \tanh \rho \\ & - \frac{\tanh \rho}{\hat{T}} \int \frac{d^3\hat{p}}{(2\pi)^3} \frac{\hat{\Delta}_{\alpha\beta}^{\mu\nu} \hat{p}^\alpha \hat{p}^\beta}{\sqrt{-g}(\hat{p}^\rho)^2} \left( \frac{p_\theta^2}{\cosh^2 \rho} + \frac{p_\phi^2}{\cosh^2 \rho \sin^2 \theta} \right) e^{-\hat{p}^\rho/\hat{T}(\rho)} \\ & - \int \frac{d^3\hat{p}}{(2\pi)^3} \frac{\hat{\Delta}_{\alpha\beta}^{\mu\nu} \hat{p}^\alpha \hat{p}^\beta}{\sqrt{-g}\hat{p}^\rho} \delta f \frac{1}{\hat{p}^\rho} \frac{\partial \hat{p}^\rho}{\partial \rho}. \end{aligned} \quad (47)$$

As already discussed, we need to work this out only for the  $\hat{\pi}^{\varsigma\varsigma}$  component. Performing the integral in the second line for  $\mu = \nu = \varsigma$  one obtains, after some algebra, its evolution equation in the following form:

$$\begin{aligned} \frac{\partial}{\partial \rho} \hat{\pi}^{\varsigma\varsigma} = & -\frac{\hat{\pi}^{\varsigma\varsigma}}{\hat{\tau}_{\text{rel}}} + \frac{4}{3} \frac{\hat{\eta}}{\hat{\tau}_{\text{rel}}} \tanh \rho - \frac{46}{21} \hat{\pi}^{\varsigma\varsigma} \tanh \rho \\ & + \frac{\tanh \rho}{3(2\pi)} \int_0^\infty d\hat{p}^\rho \int_0^{2\pi} d\theta (\hat{p}^\rho)^3 \sin \theta \left( \frac{25}{21} - \cos^2 \theta \right) (3 \cos^2 \theta - 1) \delta f. \end{aligned} \quad (48)$$

Here the second term on the r.h.s. arises from the integral over  $f_{\text{eq}}$  in (47) where we used Eq. (30), the thermodynamic relation  $\varepsilon + \mathcal{P} = \mathcal{S}T$ , and the definition  $\hat{\eta} \equiv \eta\tau^3$ . The second and last terms on the r.h.s. of Eq. (47) were rearranged, using the definition (45), to give the last two terms in Eq. (48).

The first line of Eq. (48) gives the second order conformal IS evolution equation for the independent shear viscous component (details of the derivation of the second order viscous hydrodynamical approximations are found in App. A). The second line is a correction arising from the exact treatment of the distribution function. It is precisely this type of correction that can be missed when an approximate method is used to solve the Boltzmann equation. In

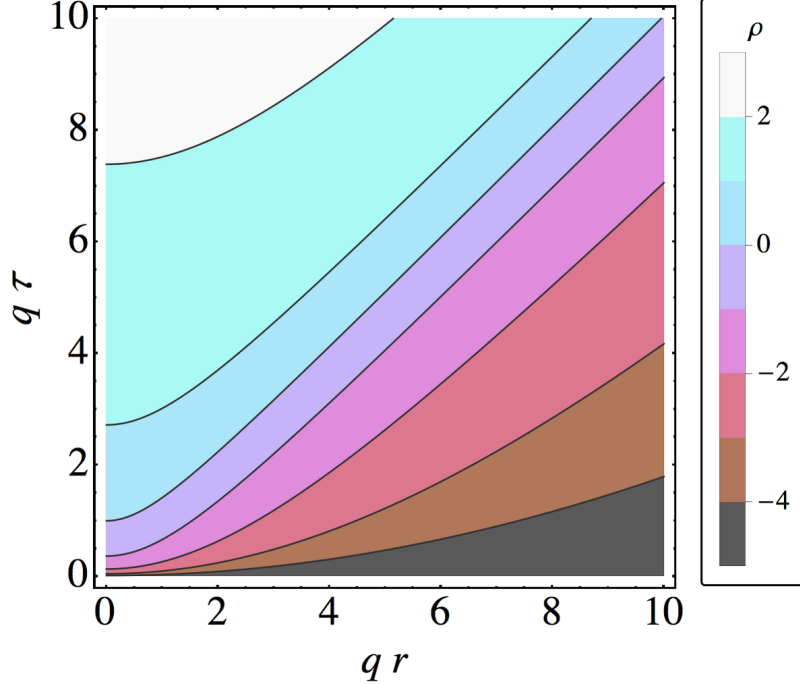


FIG. 1: (Color online) Lines of constant  $\rho$  in the  $(q\tau, qr)$  plane. The origin in de Sitter time,  $\rho = 0$ , corresponds to the line going through  $(q\tau, qr) = (1, 0)$  and the upper right corner of the graph.

Sec. V we will study how large these deviations are by comparing the exact kinetic solution with predictions from ideal and different variants of second-order viscous hydrodynamics that were obtained from the Boltzmann equation using different approximation schemes. Finally, we note that the first-order NS solution is easily extracted from Eq. (48) by taking the limit  $\hat{\tau}_{\text{rel}} \rightarrow 0$ :

$$\hat{\pi}_{NS}^{\text{ss}} = \frac{4}{3}\eta \tanh \rho. \quad (49)$$

This is precisely the exact solution to conformal NS theory previously obtained in [13, 14].

## V. RESULTS AND DISCUSSION

In this section we present solutions to Eq. (34). To obtain the solutions we first numerically solve the integral equation for the effective temperature (43) using the method of iteration [19–21]. One key difference from the exact solutions obtained previously in [19–21] is that one must solve Eq. (43) for both positive and negative values of the de Sitter time  $\rho$ . In addition, another key conceptual difference is that, instead of providing an initial condition as a function of the radius at fixed proper-time, we must instead specify an initial

condition at a fixed de Sitter time  $\rho_0$  which maps to a line in  $\tau$  and  $r$  in Milne coordinates (shown in Fig. 1).<sup>10</sup> Here we choose the initial condition at  $\rho_0$  to be isotropic and ideal, *i.e.* we require that the shear-stress tensor vanishes at  $\rho_0$ . The code necessary to obtain the exact numerical solution is included as an additional file in the arXiv version of this paper.

For the numerical solution we discretize  $\rho$  on an equally-spaced lattice from  $-\rho_{\max}$  to  $+\rho_{\max}$  with  $\rho_{\max} = 10$ . The number of grid points required depends on  $\eta/\mathcal{S}$ . For  $4\pi\eta/\mathcal{S} = 0.1$  one needs on the order of 2000 grid points and on the order of 200 iterations; however, for larger  $\eta/\mathcal{S}$  it is possible to use fewer grid points, and convergence can be achieved in a much fewer number of iterations. For the initial guess for the solution used in the iterations, we choose the ideal hydrodynamics solution of Gubser and then iterate until the energy density converges to one part in  $10^{10}$  at all points on the lattice. Once the effective temperature is obtained, it is used to compute the shear-stress, the full distribution function, and other observables, based on the results derived in the previous sections.

In what follows we will compare our numerical results with the free streaming result and three hydrodynamical approximations: the ideal solution of Gubser, the IS second-order viscous hydrodynamics solution of Ref. [15], and a (new) complete second-order viscous solution which we label as DNMR. The exact free streaming result, which corresponds to the limit  $\eta/\mathcal{S} \rightarrow \infty$  ( $c \rightarrow \infty$ ), can be obtained for both the de Sitter space temperature profile and the  $\varsigma\varsigma$  component of the shear-stress tensor using Eqs. (43) and (40a), respectively. The results are

$$\hat{T}_{\text{free streaming}}(\rho) = \mathcal{H}^{1/4} \left( \frac{\cosh \rho_0}{\cosh \rho} \right) \hat{T}_0(\rho_0), \quad (50)$$

with  $\mathcal{H}$  defined in Eq. (38), and

$$\hat{\pi}_{\text{free streaming}}^{\varsigma\varsigma}(\rho) = \mathcal{A} \left( \frac{\cosh \rho}{\cosh \rho_0} \right) \frac{\hat{T}_0^4}{\pi^2}, \quad (51)$$

with  $\mathcal{A}$  defined in Eq. (41).

In the other limit  $\eta/\mathcal{S} \rightarrow 0$  ( $c \rightarrow 0$ ), which corresponds to the ideal hydrodynamics case, one has [13, 14]

$$\hat{T}_{\text{ideal}}(\rho) = \frac{\hat{T}_0}{\cosh^{2/3}(\rho)}. \quad (52)$$

---

<sup>10</sup> Due to rotational symmetry and boost-invariance, by construction we can ignore the dependence on  $\phi$  and  $\varsigma$ ; however, in reality the surface is, in fact, three-dimensional. Note that, according to Eq. (31), a fixed temperature along a line of constant  $\rho$  implies a temperature profile that decreases like  $1/\tau(r)$  as  $r$  and  $\tau$  increase.

For the second-order hydrodynamic approximation one has to solve two coupled ordinary differential equations subject to a boundary condition at  $\rho = \rho_0$ . For the IS case, the necessary equations are

$$\frac{1}{\hat{T}} \frac{d\hat{T}}{d\rho} + \frac{2}{3} \tanh \rho = \frac{1}{3} \bar{\pi}_\zeta^\zeta(\rho) \tanh \rho, \quad (53)$$

$$\frac{d\bar{\pi}_\zeta^\zeta}{d\rho} + \frac{4}{3} (\bar{\pi}_\zeta^\zeta)^2 \tanh \rho + \frac{\bar{\pi}_\zeta^\zeta}{\hat{\tau}_\pi} = \frac{4}{15} \tanh \rho, \quad (54)$$

where  $\bar{\pi}_\zeta^\zeta \equiv \hat{\pi}_\zeta^\zeta / (\hat{T} \hat{\mathcal{S}})$  and  $\hat{\tau}_\pi = 5\eta / (\mathcal{S} \hat{T})$ . One can go beyond the IS approximation presented in Ref. [15] and also include the complete second order contribution (see App. A for further details). In this case, the second equation above should be replaced by

$$\frac{d\bar{\pi}_\zeta^\zeta}{d\rho} + \frac{4}{3} (\bar{\pi}_\zeta^\zeta)^2 \tanh \rho + \frac{\bar{\pi}_\zeta^\zeta}{\hat{\tau}_\pi} = \frac{4}{15} \tanh \rho + \frac{10}{21} \bar{\pi}_\zeta^\zeta \tanh \rho. \quad (55)$$

If Eq. (55) is used, the result is labeled as DNMR.

For all cases shown in the results section we require as the boundary condition for the solution in de Sitter space that the system is ideal at  $\rho_0 = 0$  such that  $\hat{\pi}^{\mu\nu}(\rho_0) = 0$ .

### A. Solution in de Sitter coordinates

In Fig. 2 we compare the de Sitter space temperature profile  $\hat{T}(\rho)$  for the choice  $\rho_0 = 0$  with  $\hat{\varepsilon}(\rho_0) = 1$  (corresponding to  $\hat{T}_0 = (\pi^2/3)^{1/4} = 1.3468$ ) and  $\hat{\pi}^{\zeta\zeta}(\rho_0) = 0$ . The four panels (a)-(d) show the results obtained for specific shear viscosities  $4\pi\eta/\mathcal{S} = 1, 3, 10$ , and  $100$ , respectively. In each panel we show the exact kinetic result as a solid black line, the IS approximation as a red short-dashed line, the DNMR approximation as a blue long-dashed line, the ideal hydro approximation as a green dot-dashed line, and the free streaming approximation as an orange medium-dashed line. There are two salient points to make immediately regarding these figures: As  $\eta/\mathcal{S}$  is decreased one sees convergence to the ideal hydro result for positive  $\rho$ ; as  $\eta/\mathcal{S}$  is increased one observes convergence to the free streaming result for both positive and negative  $\rho$ ; however, using the boundary condition  $\hat{\pi}^{\mu\nu}(0) = 0$  one is not able to smoothly connect to the ideal limit for negative  $\rho$ . This occurs in the exact kinetic solution and in both of the second-order viscous hydrodynamic solutions. One can fix this problem by fine-tuning the value of  $\pi^{\mu\nu}(0)$ , or instead by imposing the equilibrium boundary condition at  $\rho = -\infty$ . We address this issue in more detail in App. B where we show how to smoothly connect to the ideal hydrodynamic limit. In that same Appendix we

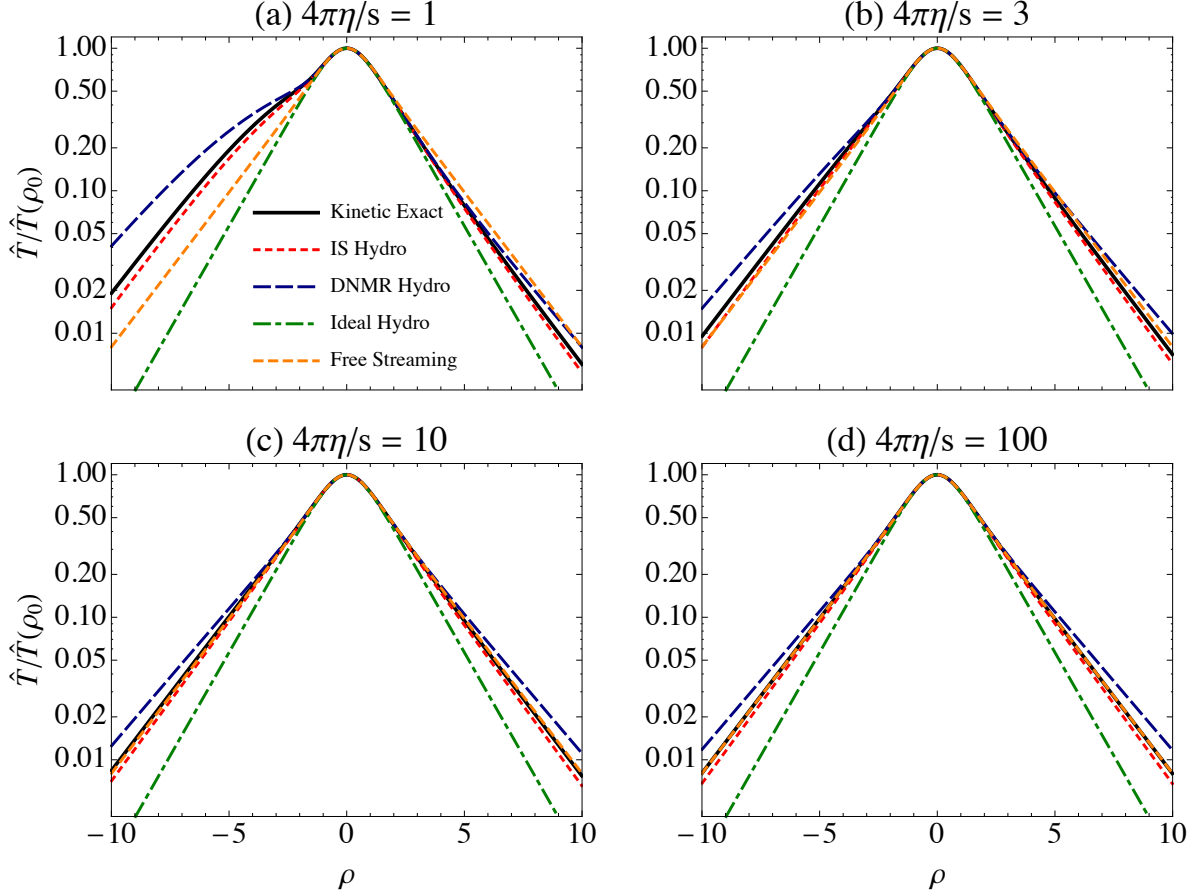


FIG. 2: (Color online) Comparison of the de Sitter space temperature profile obtained from the exact kinetic solution, ideal hydrodynamics, and two second-order formulations of viscous hydrodynamics. The four panels (a)-(d) show the results obtained assuming  $4\pi\eta/\mathcal{S} = 1, 3, 10$ , and  $100$ , respectively. In all panels we fixed  $\rho_0 = 0$  and  $\hat{\mathcal{E}}(\rho_0) = 1$ .

comment additionally on constraints that must be satisfied by the boundary conditions in order to obtain physically meaningful solutions to the kinetic equation.

Focusing next on the comparison of the second-order viscous hydrodynamic approximations to the exact kinetic solution for the de Sitter space temperature profile in Fig. 2, one sees that for values of  $\rho$  near  $\rho = 0$ , the DNMR solution agrees better with the exact kinetic solution; however, at large values of  $\rho$  (both positive and negative) we find the IS result to be the better approximation to the exact result. Finally, we note that only the exact kinetic solution is able to properly describe the largest  $\eta/\mathcal{S}$  case (Fig. 2d), which for all intents and purposes is the free streaming case.

In Fig. 3 we compare the different approximations for the de Sitter space profile of the

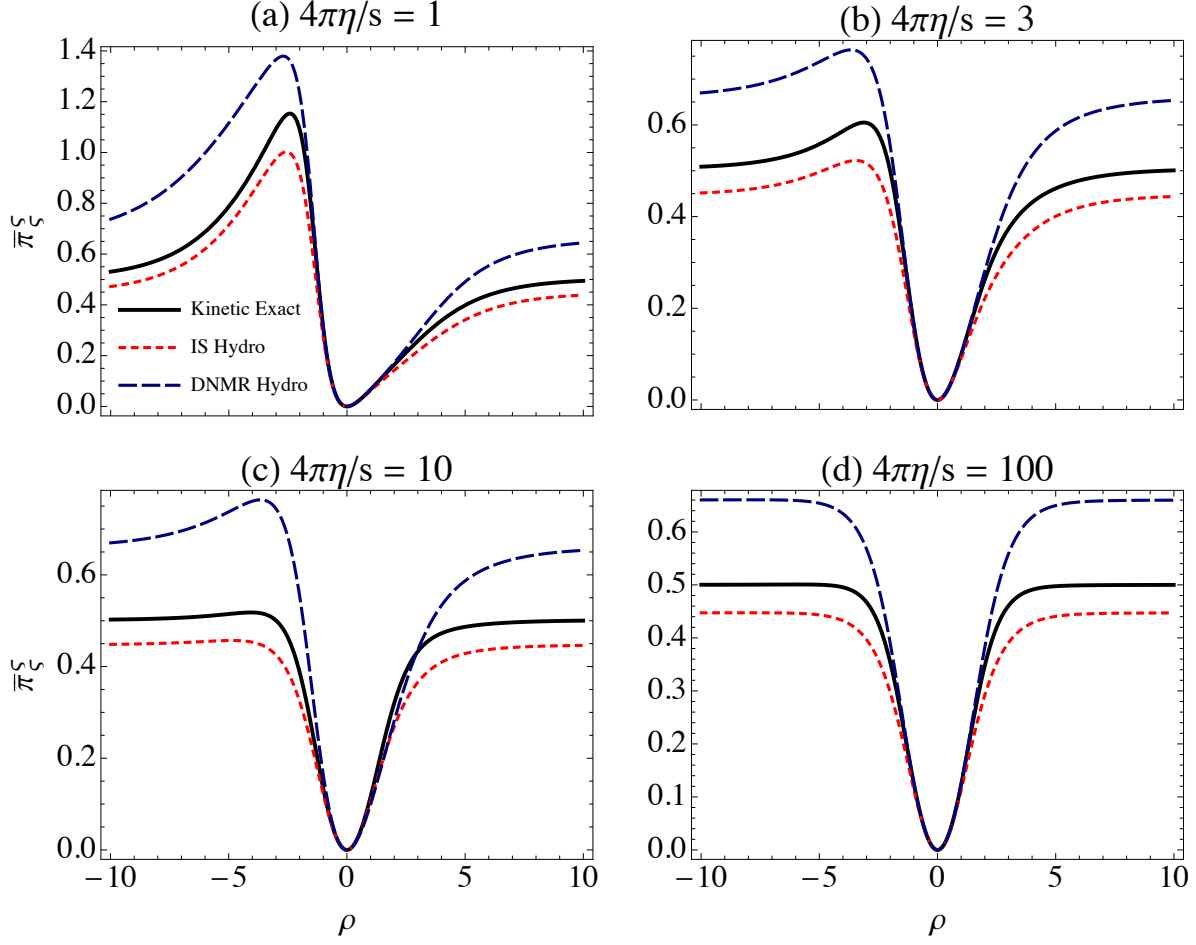


FIG. 3: (Color online) Comparison of the normalized de Sitter space shear profile  $\bar{\pi}_\zeta^\zeta \equiv \hat{\pi}_\zeta^\zeta / (\hat{T}\hat{\mathcal{S}})$  obtained from the exact kinetic solution and two second-order formulations of viscous hydrodynamics. The four panels (a)-(d) show the results obtained assuming  $4\pi\eta/\mathcal{S} = 1, 3, 10$ , and  $100$ , respectively. In all panels we fixed  $\rho_0 = 0$  and  $\hat{\mathcal{E}}(\rho_0) = 1$ .

shear stress  $\bar{\pi}_\zeta^\zeta(\rho)$ , again for the choice  $\rho_0 = 0$  with  $\hat{\mathcal{E}}(\rho_0) = 1$  and  $\bar{\pi}_\zeta^\zeta(\rho_0) = 0$ . The four panels (a)-(d) show results for four different choices of the specific shear viscosity:  $4\pi\eta/\mathcal{S} = 1, 3, 10$ , and  $100$ . In each panel we show the exact kinetic result as a solid black line, the IS hydrodynamic approximation as a short-dashed red line, and the DNMR approximation as a long-dashed blue line. As  $\eta/\mathcal{S}$  is decreased, the hydrodynamic approximations appear to approach the exact kinetic solution; however, once again, although the DNMR solution seems to agree better with the exact kinetic solution at small  $\rho$ , it appears to do a poorer job than IS at large  $\rho$ . We note, however, that one sees quite reasonable overall agreement between the exact kinetic solution and the two second-order viscous hydrodynamic solutions

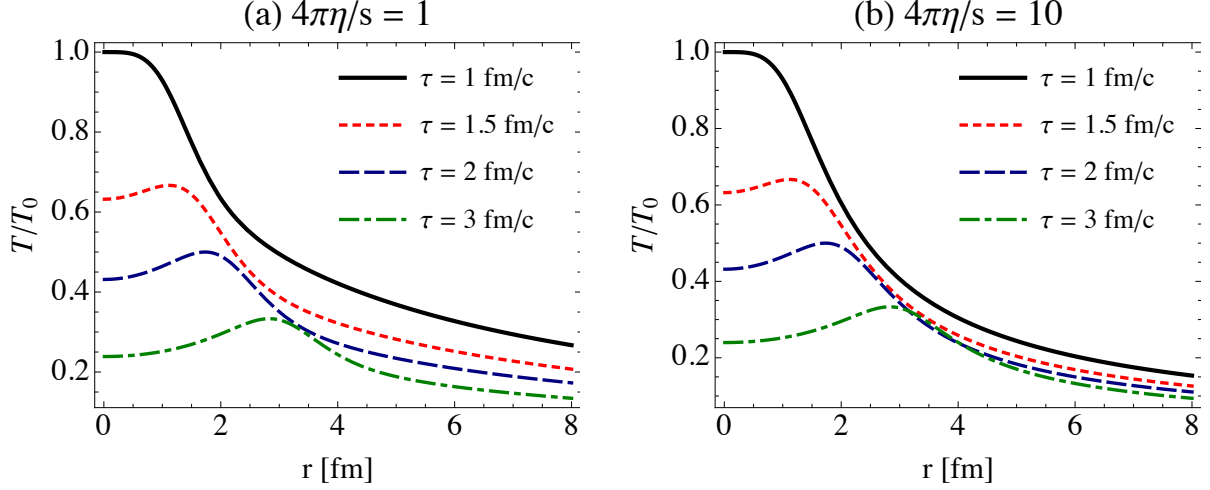


FIG. 4: (Color online) Exact solution for the proper-time evolution of the temperature profile as a function of the radial coordinate  $r$ , for  $4\pi\eta/S = 1$  in panel (a) and  $4\pi\eta/S = 10$  in panel (b)

even at extremely large values of  $\eta/S$ .

## B. Solution in Minkowski space

Once the solution in de Sitter space for  $\hat{T}$  is obtained, one can use Eqs. (4) and (31) to construct the solution in Minkowski space, mapped by  $r$  and  $\tau$  since the system is azimuthally symmetric and longitudinally boost invariant. For the purposes of this paper we present results for the case  $q = 1 \text{ fm}^{-1}$  which corresponds to a fairly small source size, with the “initial” temperature  $\hat{T}_0 \equiv \hat{T}(\rho_0=0) = 1.3468$  (from  $\hat{\varepsilon}_0 = 1$ ) translating into a temperature scale at the origin  $r = 0$  at a reference time  $\tau_0 = 1 \text{ fm}/c$  of  $T_0 \equiv T(\tau_0=1 \text{ fm}/c, r=0) \simeq 266 \text{ MeV}$ . However, all plots remain unchanged under a change of the scale  $q$  if we substitute  $r [\text{fm}] \rightarrow qr$  and  $\tau [\text{fm}/c] \rightarrow q\tau$ . The de Sitter space results shown in Figs. 2 and 3 can thus be used for any  $q$  and therefore describe an entire family of exact solutions to the RTA Boltzmann equation and their associated hydrodynamic expansions with varying source size. The choice of  $q$  affects the range of  $\rho$  to be explored in order to cover a given region in  $r$  which increases for larger  $q$  values. Viscous corrections, and differences between the exact microscopic and the approximate macroscopic evolutions will be bigger at large values of  $\rho - \rho_0$ .

In Fig. 4 we show snapshots of the radial temperature profile at four different proper times, for  $4\pi\eta/S = 1$  in panel (a) and  $4\pi\eta/S = 10$  in panel (b). One sees that changing

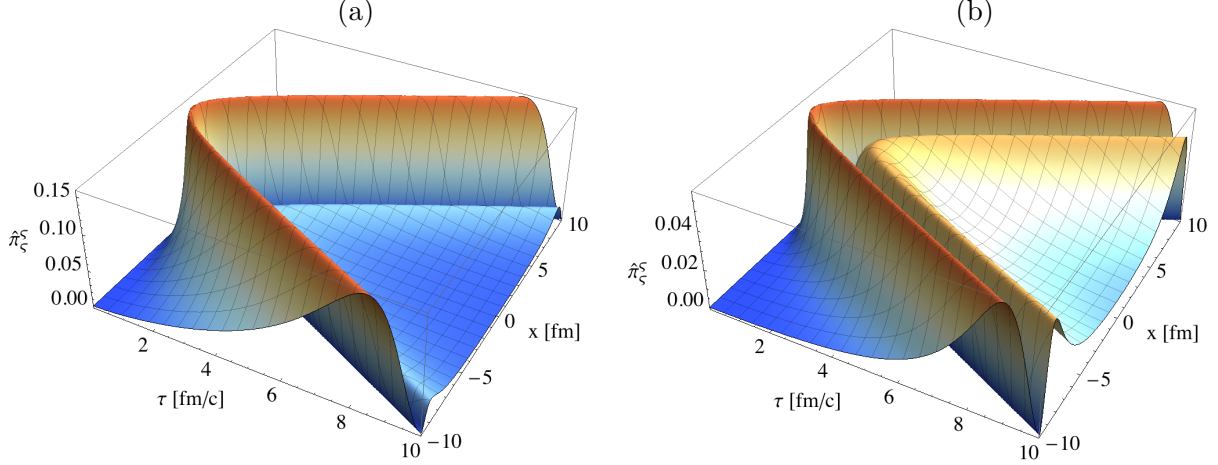


FIG. 5: (Color online) Two-dimensional slice of the spatial and proper-time evolution of the unitless shear stress  $\hat{\pi}_\xi^\xi = \tau^4 \pi_\xi^\xi$ , for  $4\pi\eta/S = 1$  in panel (a) and  $4\pi\eta/S = 10$  in panel (b).

the shear viscosity by an order of magnitude does not seem to have a strong effect on the evolution of the matter near the center (for  $r \lesssim 3 \text{ fm}/c$ ). However, at larger radii one notices an appreciable difference: for larger shear viscosity the temperature decreases more rapidly at large  $r$ . We note, however, that the weak dependence on the assumed value of  $\eta/S$  partly stems from the fact that the flow velocity profile is here constrained by the Gubser symmetry to be always the same, irrespective of the value of  $\eta/S$ .

The Minkowski space evolution of the unitless shear stress  $\hat{\pi}_\xi^\xi = \tau^4 \pi_\xi^\xi$  is graphed as a function of  $r$  and  $\tau$  in Fig. 5, for the exact solution of the Boltzmann equation with two different values of the specific shear viscosity. Note that the vertical scale changes between panels (a) and (b). Clearly, the assumed value of  $\eta/S$  has a strong effect on the spacetime evolution of the shear stress.

Finally, we compare in Fig. 6 (for  $\eta/S = 1/(4\pi)$ ) and Fig. 7 (for  $\eta/S = 10/(4\pi)$ ) snapshots of the Minkowski space temperature profile obtained from the exact kinetic solution (solid black line) with different hydrodynamic approximations: ideal hydrodynamics (dot-dashed green line), second-order IS viscous hydrodynamics (red short-dashed line), and the DNMR approximation to second-order viscous hydrodynamics (long-dashed blue line). In the top set of panels we show radial profiles at three different longitudinal proper times,  $\tau = 1, 5$ , and  $10 \text{ fm}/c$ . In the bottom set of panels we show the ratio between the temperatures corresponding to the exact kinetic result and those of the two second-order viscous hydrodynamic approximations. Note that even at the reference time  $\tau_0 = 1 \text{ fm}/c$  the temperature profiles



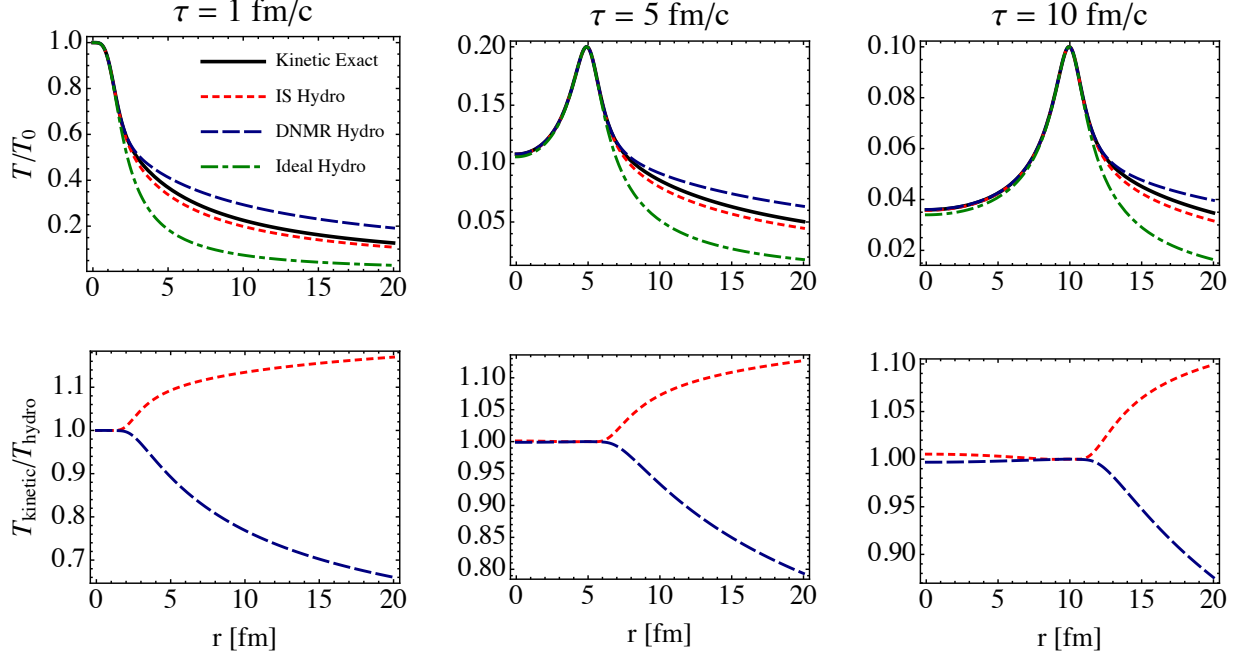


FIG. 6: (Color online) Snapshots of the temperature profile in Milne coordinates obtained from the exact kinetic solution (solid black line), ideal hydrodynamics (dot-dashed green line), the second-order IS solution (red short-dashed line), and the second-order DNMR solution (long-dashed blue line). For this figure we assumed  $4\pi\eta/\mathcal{S} = 1$ .

are not the same: since we impose initial conditions not at a fixed longitudinal proper time in Minkowski space, but at a fixed “de Sitter time”  $\rho_0$ , there is nothing special about the time  $\tau = 1 \text{ fm}/c$  (except that it is the natural longitudinal proper time scale for a scale parameter  $q = 1 \text{ fm}^{-1}$ ). Figs. 6 and 7 show that the temperatures corresponding to the exact and approximate solutions always agree at their peak value, and that the position of this peak (which corresponds to the initial value  $\rho_0 = 0$  in de Sitter space) moves out in the radial direction along the line  $r = \sqrt{\tau^2 - 1}$  as  $\tau$  increases (see Eq. (4a)).

From Fig. 6 we see that for  $4\pi\eta/\mathcal{S} = 1$  the maximum error in the temperature from the IS approach is on the order of 10-15% in the  $(\tau, r)$  region shown in the plots, and somewhat larger for the DNMR approximation. Somewhat counterintuitively, Fig. 7 seems to show a significantly smaller error for a 10 times larger shear viscosity. However, more careful inspection reveals that this is only the case to the right of the peak, which corresponds to negative  $\rho$  values; in the central region ( $r \lesssim \sqrt{\tau^2 - 1}$ ) which corresponds to positive  $\rho$  values, the late-time differences between the exact kinetic solution and the second-order viscous

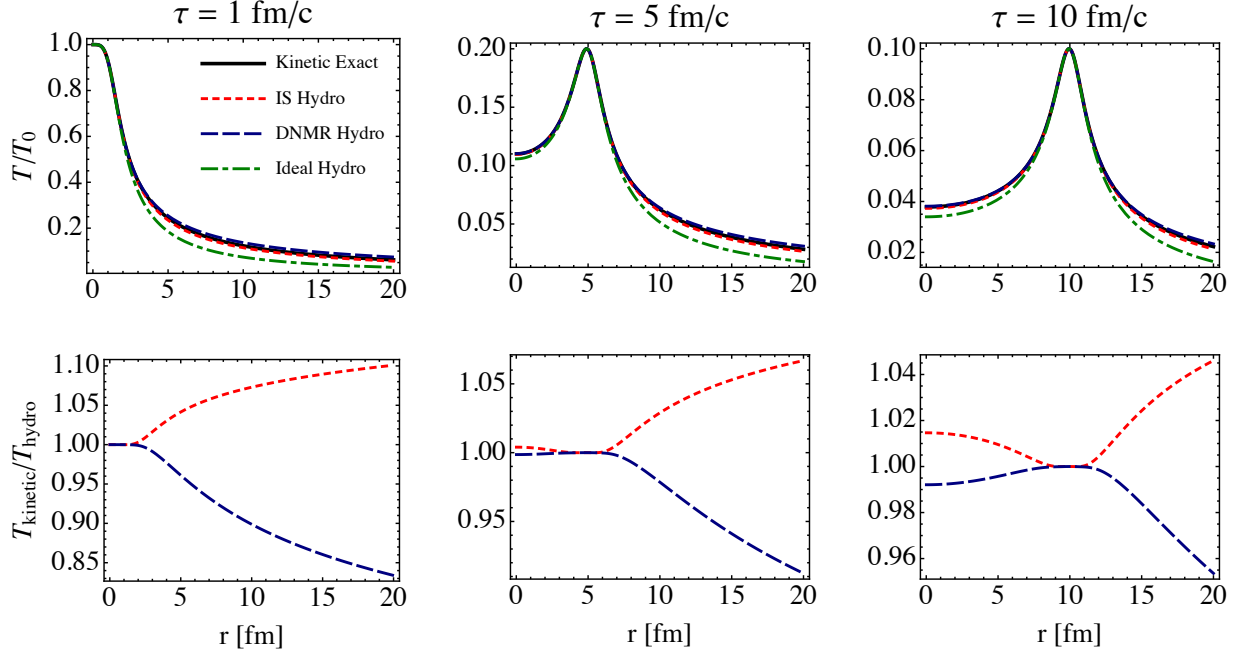


FIG. 7: (Color online) Same as Fig. 6, but for  $4\pi\eta/\mathcal{S} = 10$ .

hydrodynamic approaches *increase* with increasing  $\eta/\mathcal{S}$ , with the DNMR approach giving slightly better agreement with the exact kinetic solution. In general, the deviations of the hydrodynamic approximations from the exact solution appear to be larger at negative than for positive  $\rho$  values; this agrees qualitatively with the pattern observed in Figs. 2 and 3. Not surprisingly, the ideal hydrodynamic approximation fares worst in all cases.

## VI. CONCLUSIONS

In this paper we presented an exact solution of the Boltzmann equation in the relaxation time approximation for a system that expands with Gubser symmetric longitudinal and transverse flow. We showed that, in the conformal (massless) limit, the Boltzmann equation has an emergent Weyl symmetry. Transforming to de Sitter coordinates and imposing the Gubser flow as the four-velocity profile as well as other constraints imposed by the Gubser symmetry on the allowed dependences of the distribution function on the phase-space coordinates, we were able to cast the Boltzmann equation into stationary form. This allowed us to solve it in the form of one-dimensional integral equations for the full distribution function, temperature profile, and all components of the energy-momentum tensor. From these integral equations we could analytically extract the ideal hydrodynamic solution, several

variants of second-order viscous hydrodynamic solutions, and the free-streaming solution.

The resulting one-dimensional integral equations were then solved numerically using an iterative method which allowed us to obtain an exact solution to the kinetic equation to arbitrary numerical accuracy in de Sitter space. The resulting exact de Sitter space solution can be analytically mapped back to Minkowski space and can be used to describe an entire family of exact solutions in this space with varying physical source size. For a given source size corresponding to the choice  $q = 1 \text{ fm}^{-1}$ , we then made quantitative comparisons between the different hydrodynamic approximations and the exact kinetic solution. We found that, while not perfect, the second-order hydrodynamic approximations gave reasonable results even in the limit of large specific shear viscosities  $\eta/\mathcal{S}$ .

One complication in these comparisons is that, in order to preserve the Gubser symmetry, initial conditions must be implemented at constant “de Sitter time”  $\rho$  in de Sitter space. When mapped back to Minkowski space, one cannot guarantee that the exact and approximate solutions have the same radial temperature profile at a fixed longitudinal proper time. While this introduces some subtleties into the interpretation of the comparisons, it does not detract from the fact that one is now able to construct exact solutions to the Boltzmann equation for systems that feature simultaneous (albeit still highly symmetric) longitudinal and transverse expansion, irrespective of the assumed value of  $\eta/\mathcal{S}$  (or, equivalently, the relaxation time  $\tau_{\text{rel}}$ ). Looking forward, it will be interesting to compare the solutions described in this work with higher-order truncations of viscous hydrodynamics and with anisotropic hydrodynamics. Moreover, using similar techniques it should be possible to find additional exact solutions to the Boltzmann equation for other relativistically expanding systems (featuring e.g. transversally anisotropic (2+1)-dimensional flow) by considering more general conformal maps between Minkowski space and other curved spacetimes [16, 17]. We leave this for future work.

## Acknowledgments

M.M. thanks G. Chirilli, J. McEwen, and Z.L. Carson for useful discussions on topics related to differential geometry and conformal field theory. G.S. Denicol was supported by a Banting Fellowship from the Natural Sciences and Engineering Research Council of Canada. U.H. and M.M. were supported by the U.S. Department of Energy, Office of Science, Office

of Nuclear Physics under Award No. DE-SC0004286. J.N. thanks the Conselho Nacional de Desenvolvimento Científico e Tecnológico (CNPq) and Fundação de Amparo à Pesquisa do Estado de São Paulo (FAPESP) for support. U.H. and M.S. were supported in part (in the framework of the JET Collaboration) by U.S. DOE Awards No. DE-SC0004104 and DE-AC0205CH11231. M.S. would also like to thank the Institute for Theoretical Physics, Johann Wolfgang Goethe-Universität, Frankfurt, and the Institute for Theoretical Physics, Technische Universität Wien, for hosting him during the final stages of this project. Finally, U.H., M.M. and J.N. acknowledge support through a bilateral scientific exchange program between the Office of Sponsored Research at The Ohio State University and FAPESP.

## Appendix A: Conformal hydrodynamics

In this Appendix we derive the fluid-dynamical equations of motion in de Sitter coordinates with the metric  $\hat{g}_{\mu\nu} = \text{diag}(-1, \cosh^2 \rho, \cosh^2 \rho \sin^2 \theta, 1)$ . In these coordinates our system is static, *i.e.*  $\hat{u}_\mu = (-1, 0, 0, 0)$ , and the equations of motion simplify considerably and can be solved with little numerical effort. The nonzero components of the Christoffel symbol in these coordinates are  $\hat{\Gamma}_{\theta\theta}^\rho = \cosh \rho \sinh \rho$ ,  $\hat{\Gamma}_{\phi\phi}^\rho = \cosh \rho \sinh \rho \sin^2 \theta$ ,  $\hat{\Gamma}_{\rho\theta}^\theta = \hat{\Gamma}_{\theta\rho}^\theta = \hat{\Gamma}_{\rho\phi}^\phi = \tanh \rho$ ,  $\hat{\Gamma}_{\phi\phi}^\theta = -\sin \theta \cos \theta$ , and  $\hat{\Gamma}_{\theta\phi}^\phi = \hat{\Gamma}_{\phi\theta}^\phi = \cot \theta$ . Also, the determinant of the metric is  $\sqrt{-\hat{g}} = \cosh^2 \rho \sin \theta$ .

The expansion rate  $\hat{\theta} = \hat{\nabla}_\mu \hat{u}^\mu$  is therefore given by

$$\hat{\theta} = \frac{1}{\sqrt{-\hat{g}}} \hat{\partial}_\mu (\sqrt{-\hat{g}} \hat{u}^\mu) = 2 \tanh \rho \quad (\text{A1})$$

( $\hat{\nabla}_\mu$  is the general relativistic covariant derivative in de Sitter coordinates), while the shear tensor  $\hat{\sigma}_{\mu\nu} = \hat{\Delta}_{\mu\nu}^{\alpha\beta} \hat{\nabla}_\alpha \hat{u}_\beta$  can be shown to be

$$\hat{\sigma}_{\mu\nu} = \hat{\Gamma}_{\mu\nu}^\rho - \frac{1}{3} \hat{\Delta}_{\mu\nu} \hat{\theta} = \text{diag} \left( 0, \frac{1}{3} \cosh \rho \sinh \rho, \frac{1}{3} \sin^2 \theta \cosh \rho \sinh \rho, -\frac{2}{3} \tanh \rho \right). \quad (\text{A2})$$

The projection operators  $\hat{\Delta}_{\mu\nu}$  and  $\hat{\Delta}_{\mu\nu}^{\alpha\beta}$  were defined in the main text of the paper.

The energy conservation equation can then be re-expressed as

$$\hat{u}^\mu \hat{\nabla}_\mu \hat{\varepsilon} + (\hat{\varepsilon} + \hat{\mathcal{P}}) \hat{\nabla}_\mu \hat{u}^\mu + \hat{\pi}^{\mu\nu} \hat{\sigma}_{\mu\nu} = 0 \implies \partial_\rho \hat{\varepsilon} + 2(\hat{\varepsilon} + \hat{\mathcal{P}}) \tanh \rho - \hat{\pi}_\zeta^\zeta \tanh \rho = 0, \quad (\text{A3})$$

where we used the tracelessness  $\hat{\pi}_\mu^\mu = 0$ . Since for a conformal fluid  $\hat{\varepsilon} \sim \hat{T}^4$ , one can rewrite this equation as an equation of motion for the temperature:

$$\frac{1}{\hat{T}} \partial_\rho \hat{T} = -\frac{2}{3} \tanh \rho + \frac{1}{3} \frac{\hat{\pi}^{\zeta\zeta}}{\hat{\varepsilon} + \hat{\mathcal{P}}} \tanh \rho. \quad (\text{A4})$$

The equation for the shear stress tensor is written as

$$\hat{\tau}_\pi \hat{\Delta}_{\mu\nu}^{\alpha\beta} \hat{u}^\lambda \hat{\nabla}_\lambda \hat{\pi}_{\alpha\beta} + \hat{\pi}_{\mu\nu} = -2\hat{\eta} \hat{\sigma}_{\mu\nu} - \frac{4}{3} \hat{\pi}_{\mu\nu} \hat{\theta} - \frac{10}{7} \hat{\pi}_{\langle\mu}^\lambda \hat{\sigma}_{\nu\rangle\lambda}. \quad (\text{A5})$$

The term  $\hat{\pi}_{\langle\mu}^\lambda \hat{\sigma}_{\nu\rangle\lambda}$  can be simplified as follows:

$$\hat{\pi}_{\langle\mu}^\lambda \hat{\sigma}_{\nu\rangle\lambda} = \Delta_{\mu\nu}^{\alpha\beta} \hat{\pi}_\alpha^\lambda \hat{\sigma}_{\beta\lambda} = \frac{1}{2} \hat{\pi}_\mu^\lambda \hat{\sigma}_{\nu\lambda} + \frac{1}{2} \hat{\pi}_\nu^\lambda \hat{\sigma}_{\mu\lambda} + \frac{1}{3} \hat{\Delta}_{\mu\nu} \hat{\pi}^{\zeta\zeta} \tanh \rho, \quad (\text{A6})$$

where

$$\begin{aligned} \hat{\pi}_{\langle\zeta}^\lambda \hat{\sigma}_{\rangle\lambda} &= -\frac{1}{3} \hat{\pi}_\zeta^\zeta \tanh \rho, \\ \hat{\pi}_{\langle\theta}^\lambda \hat{\sigma}_{\rangle\lambda} &= -\frac{1}{3} \cosh \rho \sinh \rho \hat{\pi}_\phi^\phi, \\ \hat{\pi}_{\langle\phi}^\lambda \hat{\sigma}_{\rangle\lambda} &= \frac{1}{3} \cosh \rho \sinh \rho \sin^2 \theta \hat{\pi}_\theta^\theta. \end{aligned} \quad (\text{A7})$$

The relaxation term  $\hat{\Delta}_{\mu\nu}^{\alpha\beta} \hat{u}^\lambda \hat{\nabla}_\lambda \hat{\pi}_{\alpha\beta}$  is worked out as

$$\hat{\Delta}_{\mu\nu}^{\alpha\beta} \hat{u}^\lambda \hat{\nabla}_\lambda \hat{\pi}_{\alpha\beta} = \hat{D} \hat{\pi}_{\mu\nu} - \hat{\pi}_{\alpha\beta} \hat{D} \hat{\Delta}_{\mu\nu}^{\alpha\beta}, \quad (\text{A8})$$

where  $\hat{D} = \hat{u}^\lambda \hat{\nabla}_\lambda$ . The first term on the right is given by

$$\hat{D} \hat{\pi}_{\mu\nu} = \hat{u}^\lambda \hat{\nabla}_\lambda \hat{\pi}_{\mu\nu} = \hat{u}^\lambda \hat{\partial}_\lambda \hat{\pi}_{\mu\nu} - \hat{u}^\lambda \hat{\Gamma}_{\mu\lambda}^\alpha \hat{\pi}_{\alpha\nu} - \hat{u}^\lambda \hat{\Gamma}_{\nu\lambda}^\alpha \hat{\pi}_{\alpha\mu} \quad (\text{A9})$$

while the second one is

$$-\hat{\pi}_{\alpha\beta} \hat{D} \hat{\Delta}_{\mu\nu}^{\alpha\beta} = -\hat{\pi}_{\alpha\beta} \hat{D} (\hat{\Delta}_\mu^\alpha \hat{\Delta}_\nu^\beta) = (\hat{u}_\nu \hat{\pi}_\mu^\alpha + \hat{u}_\mu \hat{\pi}_\nu^\alpha) \hat{u}^\sigma \hat{\Gamma}_{\sigma\alpha}^\lambda \hat{u}_\lambda. \quad (\text{A10})$$

Thus, the equations of motion for  $\hat{\pi}_{\theta\theta}$ ,  $\hat{\pi}_{\phi\phi}$ , and  $\hat{\pi}_{\zeta\zeta}$  become

$$\hat{\tau}_\pi \partial_\rho \hat{\pi}_{\theta\theta} + \hat{\pi}_{\theta\theta} = - \left( \frac{2}{3} \hat{\eta} \cosh^2 \rho + \frac{2}{3} \hat{\tau}_\pi \hat{\pi}_{\theta\theta} + \frac{10}{21} \frac{\hat{\tau}_\pi \hat{\pi}_{\phi\phi}}{\sin^2 \theta} \right) \tanh \rho, \quad (\text{A11})$$

$$\hat{\tau}_\pi \partial_\rho \hat{\pi}_{\phi\phi} + \hat{\pi}_{\phi\phi} = - \left( \frac{2}{3} \hat{\eta} \cosh^2 \rho \sin^2 \theta + \frac{2}{3} \hat{\tau}_\pi \hat{\pi}_{\phi\phi} + \frac{10}{21} \hat{\tau}_\pi \hat{\pi}_{\theta\theta} \sin^2 \theta \right) \tanh \rho, \quad (\text{A12})$$

$$\hat{\tau}_\pi \partial_\rho \hat{\pi}_{\zeta\zeta} + \hat{\pi}_{\zeta\zeta} = \left( \frac{4}{3} \hat{\eta} - \frac{8}{3} \hat{\tau}_\pi \hat{\pi}_{\zeta\zeta} + \frac{10}{21} \hat{\pi}_{\zeta\zeta} \right) \tanh \rho. \quad (\text{A13})$$

One sees that  $\hat{\pi}_{\zeta\zeta}$  decouples while the remaining two components of the shear stress are coupled to each other. Due to the tracelessness of the shear stress tensor it is, however, sufficient to only solve the last equation, Eq. (A13).

Defining the scaled shear stress  $\bar{\pi}_\zeta^\zeta = \hat{\pi}_\zeta^\zeta / (\hat{\varepsilon} + \hat{\mathcal{P}})$  and using the fact that in massless kinetic theory  $\hat{\eta} / \hat{\tau}_\pi = (\hat{\varepsilon} + \hat{\mathcal{P}}) / 5$ , we arrive after a few more steps at the following final form of the equations of motion in de Sitter coordinates:

$$\frac{1}{\hat{T}} \partial_\rho \hat{T} + \frac{2}{3} \tanh \rho = \frac{1}{3} \bar{\pi}_\zeta^\zeta \tanh \rho, \quad (\text{A14})$$

$$\partial_\rho \bar{\pi}_\zeta^\zeta + \frac{\bar{\pi}_\zeta^\zeta}{\hat{\tau}_\pi} \tanh \rho + \frac{4}{3} (\bar{\pi}_\zeta^\zeta)^2 = \frac{4}{15} \tanh \rho + \frac{10}{7} \bar{\pi}_\zeta^\zeta \tanh \rho. \quad (\text{A15})$$

In traditional Israel-Stewart theory [15], where the term proportional to  $\hat{\pi}_{\langle\mu}^\lambda \hat{\sigma}_{\nu\rangle\lambda}$  is absent, the equation of motion for  $\hat{\pi}^{\zeta\zeta}$  reduces to

$$\partial_\rho \bar{\pi}_\zeta^\zeta + \frac{\bar{\pi}_\zeta^\zeta}{\hat{\tau}_\pi} \tanh \rho + \frac{4}{3} (\bar{\pi}_\zeta^\zeta)^2 = \frac{4}{15} \tanh \rho. \quad (\text{A16})$$

The last three equations are Eqs. (53)-(55) in Sec. V.

## Appendix B: Physical constraints on the de Sitter space boundary condition

As mentioned in the body of this paper, in order to obtain the exact solution to the kinetic equation one must specify an initial condition in de Sitter space. The exact kinetic solution obtained herein assumed  $\hat{\pi}_\zeta^\zeta(\rho_0) = 0$  at some particular value  $\rho_0$ . In the Sec. V we chose  $\rho_0 = 0$  in order to make the comparison between the various approaches most transparent, however, one has some degree of freedom in the choice of this parameter. One issue with the solutions presented in the main body is that it is not possible to take the limit  $\eta/\mathcal{S} \rightarrow 0$  in order to recover the ideal hydrodynamics limit (see Fig. 2). As can be seen from Fig. 2, for negative  $\rho$  the solution does not converge to the ideal hydrodynamic limit as  $\eta/\mathcal{S} \rightarrow 0$ . In fact, for very small values of  $\eta/\mathcal{S}$  one finds that the solution diverges at some finite negative  $\rho$ . This behavior is not restricted to the exact kinetic solution and occurs within both the IS and DNMR second-order viscous hydrodynamic approaches as well.

In order to take the small  $\eta/\mathcal{S}$  limit, one must very carefully take  $\eta/\mathcal{S} \rightarrow 0$  using a positive value of  $\hat{\pi}_\zeta^\zeta(0)$  which vanishes only when  $\eta/\mathcal{S}$  is precisely zero. For the IS and DNMR second-order viscous hydrodynamic solutions, one can iteratively determine the necessary value of  $\hat{\pi}_\zeta^\zeta(\rho_0)$  required to recover the ideal hydrodynamic result as  $\eta/\mathcal{S} \rightarrow 0$ ; however, due to the form of the initial distribution function assumed herein, it is not currently possible to implement a finite value for  $\hat{\pi}_\zeta^\zeta(\rho_0)$  in the exact kinetic solution. As an alternative approach which guarantees convergence to the ideal hydrodynamic result as  $\eta/\mathcal{S} \rightarrow 0$  one could instead

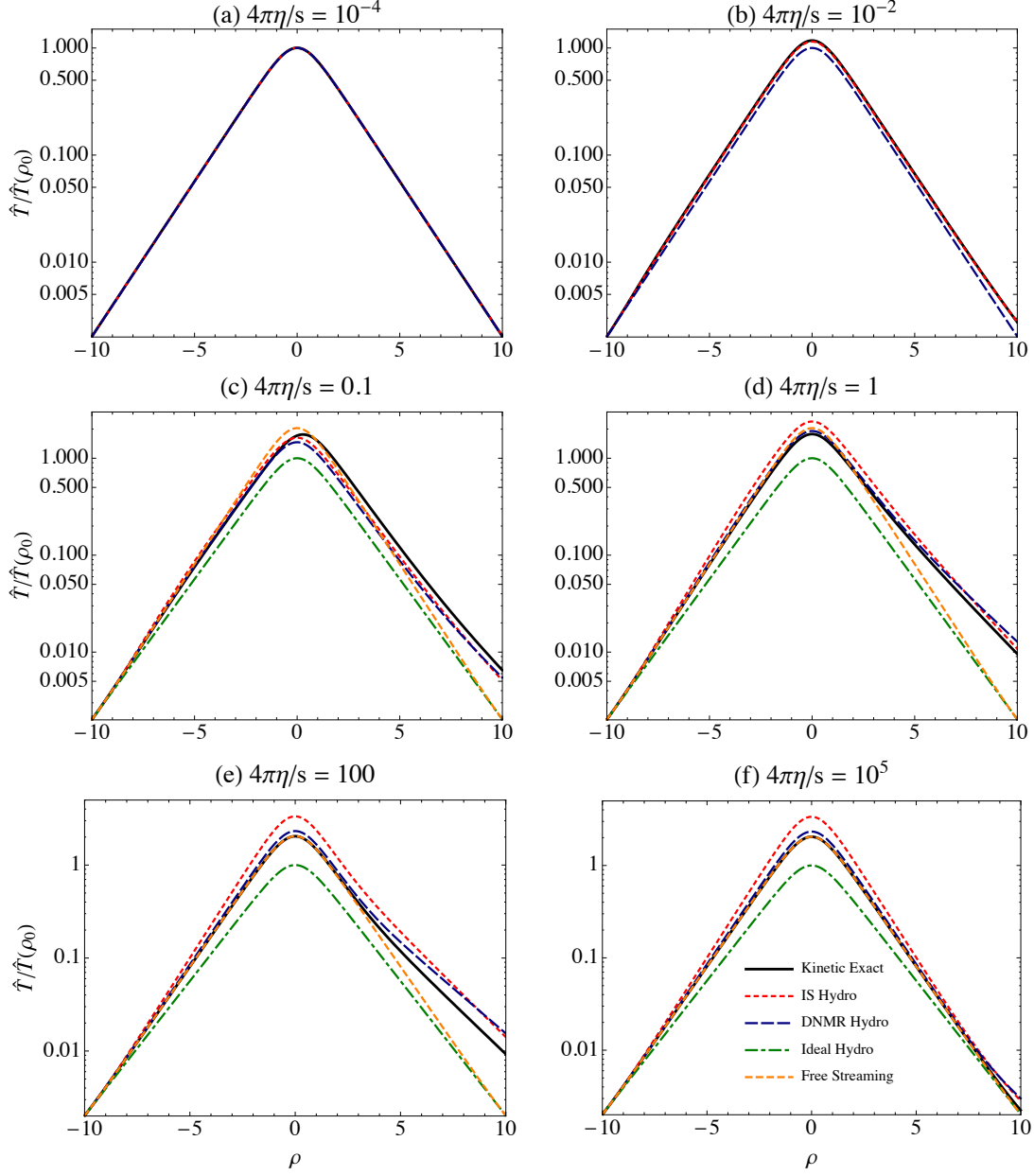


FIG. 8: (Color online) Comparison of the de Sitter space temperature profile obtained from the exact kinetic solution, ideal hydrodynamics, and two second-order formulations of viscous hydrodynamics, with equilibrium initial conditions imposed at  $\rho_0 = -10$  with  $\hat{T}(\rho_0) = 2.02018 \times 10^{-3}$ . Panels (a)-(f) show the results obtained assuming  $4\pi\eta/S = 10^{-4}$ ,  $10^{-2}$ ,  $1$ ,  $10$ ,  $100$ , and  $10^5$ , respectively.

fix the boundary condition on the left edge of the simulation region.<sup>11</sup> If this is done, one can straightforwardly take the ideal limit.

<sup>11</sup> As the simulation region is enlarged, this corresponds to fixing the boundary condition at  $\rho \rightarrow -\infty$ .

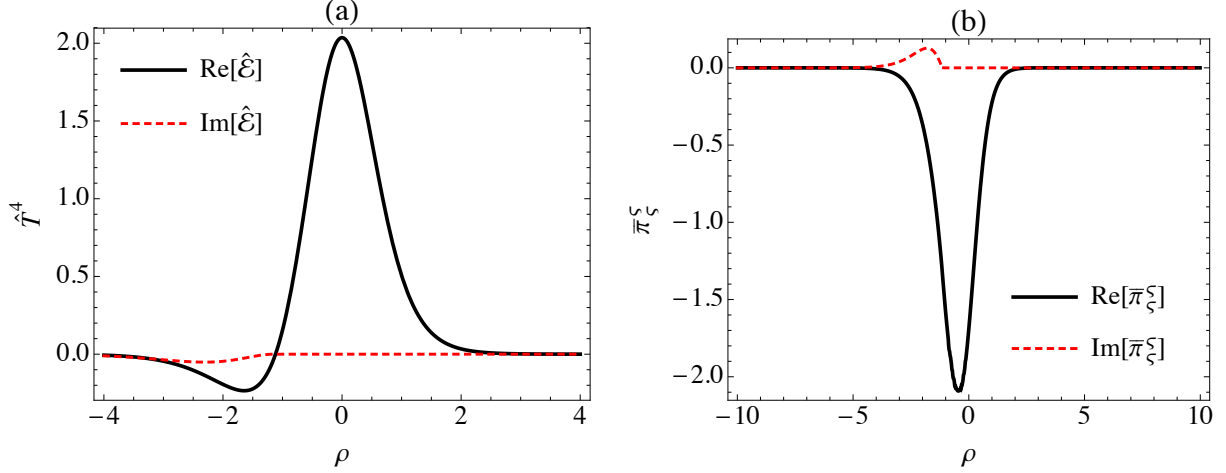


FIG. 9: (Color online) The de Sitter space temperature profile obtained from the exact kinetic solution assuming  $4\pi\eta/\mathcal{S} = 3$  and  $\rho_0 = 3$  with  $\hat{T}(\rho_0) = 0.214477$ .

To demonstrate this, in Fig. 8 we plot the results obtained with such a boundary condition for both small and large values of  $\eta/\mathcal{S}$ . For very small specific shear viscosities the exact kinetic solution is computationally very demanding and cannot be obtained with our computing resources, so in panels (a) and (b) we graph only our macroscopic solutions for ideal and viscous hydrodynamics. Panel (a) shows that, with equilibrium boundary conditions implemented at large negative de Sitter times, the two viscous hydrodynamic approximations (which in Fig. 2 are seen to bracket the exact kinetic solution at negative values of  $\rho - \rho_0$ ) perfectly reproduce the ideal fluid limit when  $\eta/\mathcal{S}$  becomes very small. Fig. 9f, on the other hand, demonstrates that for very large values of  $\eta/\mathcal{S}$  the exact kinetic solution converges perfectly to the free-streaming limit. For finite shear viscosity, however, a complication with this type of boundary condition is that by implementing it at the left edge in de Sitter space one will not find the same temperature and shear correction at positive  $\rho$  values (which in Minkowski space map to the central fireball region at times on the order of 1 fm/c). As a result, it is more difficult to make apples-to-apples comparisons of the Minkowski-space evolution in this case. It is for this reason that in the body of the text we chose the simpler “initial condition”  $\hat{\pi}_\zeta = 0$  at  $\rho_0 = 0$ . This condition guarantees that all approaches start with an isotropic initial condition that is essentially free from shear corrections near the fireball center at longitudinal proper times on the order of 1 fm/c.

We note also that, for any value of  $\eta/\mathcal{S}$  one could also attempt to initialize the system in de Sitter space in equilibrium at a positive value of  $\rho_0$ ; however, one finds in practice that



doing this can result in complex-valued energy densities and, if  $\rho_0$  is taken to be large enough, the numerical solution will fail to converge. Once again, this behavior is not unique to the kinetic solution and similar behavior can be seen in the second-order viscous hydrodynamic solutions. Of course, negative or complex energy densities are unphysical, and this numerical phenomenon indicates that the physical range of  $\rho$  values, where the distribution function corresponding to a thermal equilibrium boundary condition at  $\rho_0$  remains positive definite for all momenta, ends somewhere at sufficiently large negative values of  $\rho - \rho_0$ . We have observed this phenomenon even for  $\rho_0 = 0$  where it appears to happen at larger and larger negative values of  $\rho$  as  $\eta/\mathcal{S}$  decreases, but never completely disappears.

As a concrete illustration of this, in Fig. 9 we plot the de Sitter space profile of  $\hat{T}^4$  in panel (a) and  $\hat{\pi}_\xi^\xi$  in panel (b). In both panels, the black solid line is the real part of the quantity and the red short-dashed line is the imaginary part of the quantity. In the case shown, the code can be made to converge to arbitrary accuracy, however, the resulting solutions are complex-valued for sufficiently negative  $\rho - \rho_0$ . While this result is, in fact, a mathematical solution to the RTA Boltzmann equation subject to the Gubser flow profile, a complex temperature is physically meaningless and (we believe) indicative of deeper underlying problems related to a violation of positivity of the distribution function  $f$  at large negative  $\rho - \rho_0$ . As a minimum, one must therefore restrict the choice of  $\rho_0$  such that (a) the code converges and (b) both the temperature and shear correction remain real-valued over the entire de Sitter space domain considered.<sup>12</sup> In future work we plan to relax the requirement  $\hat{\pi}_\xi^\xi(\rho_0) = 0$  in which case it may be possible to impose initial conditions over a larger range of  $\rho_0$ , without the solutions becoming unphysical.

---

[1] P. Gressman and R. Strain, J. Amer. Math. Soc. **24**, 771 (2011).

[2] S. R. de Groot, W. A. van Leeuwen, and C. G. van Weert, *Relativistic Kinetic Theory: principles and applications* (Elsevier North-Holland, 1980).

<sup>12</sup> We caution that, since the solution for the temperature (which enters all other computed quantities) is obtained from a moment of the distribution function (see Eq. (43)), problems with the positivity of the distribution function in some parts of momentum space may not immediately signal themselves through complex temperature values. Therefore, unphysical behaviour of the distribution function may remain hidden in part of the  $\rho$  space determined by this procedure.

- [3] C. Cercignani and G. Medeiros Kremer, *The relativistic Boltzmann Equation: Theory and Applications* (Birkhäuser Verlag (Basel, Switzerland), 2002).
- [4] W. A. Hiscock and L. Lindblom, Ann. Phys. **151**, 466 (1983).
- [5] W. A. Hiscock and L. Lindblom, Phys. Rev. **D31**, 725 (1985).
- [6] W. Israel and J. M. Stewart, Ann. Phys. **118**, 341 (1979).
- [7] A. Jaiswal, Phys. Rev. **C87**, 051901 (2013), 1302.6311.
- [8] A. Jaiswal, Phys.Rev. **C88**, 021903 (2013), 1305.3480.
- [9] R. S. Bhalerao, A. Jaiswal, S. Pal, and V. Sreekanth, Phys.Rev. **C89**, 054903 (2014), 1312.1864.
- [10] G. Denicol, T. Koide, and D. Rischke, Phys.Rev.Lett. **105**, 162501 (2010), 1004.5013.
- [11] G. S. Denicol, H. Niemi, E. Molnár, and D. H. Rischke, Phys. Rev. D **85**, 114047 (2012).
- [12] G. Denicol, E. Molnar, H. Niemi, and D. Rischke, Eur. Phys. J. A **48**, 170 (2012), 1206.1554.
- [13] S. S. Gubser, Phys.Rev. **D82**, 085027 (2010), 1006.0006.
- [14] S. S. Gubser and A. Yarom, Nucl.Phys. **B846**, 469 (2011), 1012.1314.
- [15] H. Marrochio, J. Noronha, G. S. Denicol, M. Luzum, S. Jeon, et al. (2013), 1307.6130.
- [16] Y. Hatta, J. Noronha, and B.-W. Xiao, Phys.Rev. **D89**, 051702 (2014), 1401.6248.
- [17] Y. Hatta, J. Noronha, and B.-W. Xiao (2014), 1403.7693.
- [18] G. Baym, Phys. Lett. **B138**, 18 (1984).
- [19] W. Florkowski, R. Ryblewski, and M. Strickland, Nucl.Phys. **A916**, 249 (2013), 1304.0665.
- [20] W. Florkowski, R. Ryblewski, and M. Strickland, Phys. Rev. **C88**, 024903 (2013), 1305.7234.
- [21] W. Florkowski, E. Maksymiuk, R. Ryblewski, and M. Strickland (2014), 1402.7348.
- [22] J. D. Bjorken, Phys. Rev. **D27**, 140 (1983).
- [23] G. S. Denicol, U. W. Heinz, M. Martinez, J. Noronha, and M. Strickland (2014), 1408.5646.
- [24] F. Debbasch and W. van Leeuwen, Physica A: Statistical Mechanics and its Applications **388**, 1079 (2009).
- [25] F. Debbasch and W. van Leeuwen, Physica A: Statistical Mechanics and its Applications **388**, 1818 (2009).
- [26] J. Anderson and H. Witting, Physica **74**, 466 (1974).
- [27] P. L. Bhatnagar, E. P. Gross, and M. Krook, Phys. Rev. **94**, 511 (1954).
- [28] R. Baier, P. Romatschke, D. T. Son, A. O. Starinets, and M. A. Stephanov, JHEP **0804**, 100 (2008), 0712.2451.

- [29] G. Baym, Nucl.Phys. **A418**, 525C (1984).
- [30] A. Białas and W. Czyż, Phys. Rev. D **30**, 2371 (1984).
- [31] A. Białas and W. Czyż, Nuclear Physics B **296**, 611 (1988).
- [32] M. Martinez and M. Strickland, Nucl. Phys. **A848**, 183 (2010), 1007.0889.
- [33] W. Florkowski and R. Ryblewski, Phys.Rev. **C83**, 034907 (2011), 1007.0130.
- [34] R. Ryblewski and W. Florkowski, J.Phys.G **G38**, 015104 (2011), 1007.4662.
- [35] M. Martinez and M. Strickland, Nucl.Phys. **A856**, 68 (2011), 1011.3056.
- [36] R. Ryblewski and W. Florkowski, Eur.Phys.J. **C71**, 1761 (2011), 1103.1260.
- [37] W. Florkowski and R. Ryblewski, Phys.Rev. **C85**, 044902 (2012), 1111.5997.
- [38] M. Martinez, R. Ryblewski, and M. Strickland, Phys.Rev. **C85**, 064913 (2012), 1204.1473.
- [39] R. Ryblewski and W. Florkowski, Phys.Rev. **C85**, 064901 (2012), 1204.2624.
- [40] W. Florkowski, R. Maj, R. Ryblewski, and M. Strickland, Phys.Rev. **C87**, 034914 (2013), 1209.3671.
- [41] D. Bazow, U. W. Heinz, and M. Strickland (2013), 1311.6720.
- [42] W. Florkowski and R. Maj, Acta Phys.Polon. **B44**, 2003 (2013), 1309.2786.
- [43] L. Tinti and W. Florkowski, Phys.Rev. **C89**, 034907 (2014), 1312.6614.
- [44] W. Florkowski and O. Madetko (2014), 1402.2401.
- [45] W. Florkowski, R. Ryblewski, M. Strickland, and L. Tinti (2014), 1403.1223.
- [46] G. S. Denicol, J. Noronha, H. Niemi, and D. H. Rischke, Phys.Rev. **D83**, 074019 (2011), 1102.4780.